Preprint typeset using LaTeX style emulateapj v. 5/25/10

ON THE ORIGIN OF THE ANGULAR MOMENTUM PROPERTIES OF GAS AND DARK MATTER IN GALACTIC HALOS AND ITS IMPLICATIONS

SANJIB SHARMA, MATTHIAS STEINMETZ, JOSS BLAND-HAWTHORN
Sydney Institute for Astronomy, School of Physics, University of Sydney, NSW 2006, Australia
Astrophysikalisches Institut Potsdam, An der Sternwarte 16, 14482,Potsdam, Germany and
Sydney Institute for Astronomy, School of Physics, University of Sydney, NSW 2006, Australia

ABSTRACT

We perform a set of non-radiative hydrodynamical simulations of merging spherical halos in order to understand the angular momentum properties of the galactic halos seen in cosmological simulations. The universal shape of angular momentum distributions seen in cosmological simulations is found to be generically produced as a result of mergers. Since the universal shape is such that it has an excess of low angular momentum material as compared to what is needed to explain the exponential structure of disc galaxies, this means that any halo formed in a merger driven cosmology will always suffer from the above mentioned problem. A resolution to this is suggested by the spatial distribution of low angular momentum material which is found to be in the center and a conical region close to the axis of rotation. Hence a mechanism, which preferentially discards the material in the center and prevents the material along the poles from falling onto the disc, can help alleviate the problem of excess low angular momentum. Feedback from star formation or nuclear activity can naturally drive such an outflow due to the flattened geometry of the assembling gas. We studied the evolution of angular momentum in halos undergoing mergers and found that for dark matter there is an inside-out transfer of angular momentum whereas for gas there is an outside in transfer. This is because the late infalling high angular momentum gas shocks with the expanding gas in the inner regions leading to a transfer of angular momentum. For collisionless dark matter particles the late infalling high angular momentum particles simply gain more energy making them migrate towards the outer regions. This provides an explanation for the fact that, for halos in cosmological simulations, the spin parameter λ and the shape parameter α of angular momentum distributions is found to be higher for gas as compared to dark matter. The inside out transfer of angular momentum is also responsible for the apparent high spin of dark matter halos undergoing mergers. Our results suggest that much lower values of offset parameter than what is currently used would be required to reliably detect such cases. In galactic halos the angular velocity of both gas and dark matter is found to be independent of angular direction suggesting that halos can be analytically modelled as shells of matter in solid body rotation. Finally, we demonstrate that the misalignment of angular momentum between gas and dark matter only occurs when the intrinsic spins of the merging halos are not aligned with the orbital angular momentum of the system. The self misalignment (orientation of angular momentum when measured in radial shells not being constant) also occurs under similar conditions. This self misalignment could be the cause of warps in discs galaxies and could also be responsible for anomalous rotation of gas seen in some galaxies. The frequency and amplitude of this misalignment is roughly consistent with the properties of warps seen in disc galaxies.

Subject headings: methods: data analysis – methods: numerical – cosmology: dark matter–galaxies: halos–galaxies: structure

1. INTRODUCTION

In the standard picture of galaxy formation, galactic halos acquire their angular momentum via tidal torques (Peebles 1969) in the linear regime and the process lasts till about turnaround, when the system decouples from the Hubble flow. After the collapse the system forms a virialized structure. The gas inside the virialized dark matter halo then cools radiatively and collapses while conserving its angular momentum, resulting in the formation of centrifugally supported disks (White & Rees 1978; White 1984; Fall & Efstathiou 1980). The process is also accompanied by the adiabatic contraction of the dark matter halo Blumenthal et al. (1986). This standard picture leads to distribution of size and luminosity of galaxies in reasonable agreement with observations (Mo et al. 1998; Dalcanton et al. 1997; Kauffmann 1996; Avila-Reese et al. 1998; Dutton et al. 2007; van den Bosch 2000; Gnedin et al. 2007).

But detailed simulations revealed two problems. Firstly in simulations incorporating gas with cooling and star formation, the gas was found to lose a significant fraction of its angular momentum, resulting in discs which were too small in size, a problem known as the angular momentum catastrophe (Steinmetz & Navarro 1999; Navarro & Steinmetz 1997; Navarro & White 1994; Navarro & Benz 1991; Sommer-Larsen et al. 1999). The cause of the problem is that, due to efficient cooling the gas is accreted as dense clumps which during mergers lose their angular momentum via dynamical friction.

Second problem is the angular momentum distribution (AMD hereafter) problem which says that even if the angular momentum is assumed to be conserved one cannot explain the exponential nature of disc galaxies. Using cold dark matter numerical simulations, it was shown by Bullock et al. (2001) that if disks are formed from gas with angular momentum distributions similar to that of dark matter, then this results in excess mass near the center as compared to an exponential disc. Specifically there is too much low angular momentum material and this makes it very hard to explain the origin of bulgeless dwarf galaxies (van den Bosch et al. 2001; van den Bosch 2001). Simulations incorporation non-radiative gas also lead to similar conclusions (Sharma & Steinmetz 2005; van den

Bosch et al. 2002). As demonstrated in Sharma & Steinmetz (2005), the resulting angular momentum distributions written in terms of $s = j/j_{\rm tot}$ closely follows a law of form $P(s) = [\alpha^{\alpha}/\Gamma(\alpha)]s^{\alpha-1}e^{-\alpha s}$, the universal form found in dark matter halos of cosmological N-body simulations. Although the α parameter for gas is slightly higher (close to 0.9) than that of dark matter (0.83) but is still much less than $\alpha > 1.3$, which is needed for explaining the exponential structure of galactic disks.

The origin of the the universal form of the angular momentum distributions is still poorly understood and if we can understand it, that might provide the clue to solving the problem. Maller & Dekel (2002) proposed a model of build up of angular momentum by a sequence of mergers. In this model, the final halo spin is assumed to be the sum of orbital angular momenta of merging satellites. The model was found to correctly reproduce the distribution of spin parameters of halos (Vitvitska et al. 2002; Maller et al. 2002). A simple extension of this model was also found to roughly reproduce the angular momentum distributions. According to this model, the magnitude and direction of the total angular momentum of a halo is predominantly determined by the last major merger and hence the major merger contributes to the high angular momentum part of the AMD. The numerous small satellites fall in from random directions and mainly contribute to the low angular momentum part of the AMD. This suggests that blowout of gas, e.g., by means of supernova feedback, from small halos can eliminate the low angular momentum part of the distribution and might resolve the angular momentum distribution problem in addition to the angular momentum catastrophe problem (Steinmetz & Navarro 1999; Navarro & Steinmetz 1997; Navarro & White 1994; Navarro & Benz 1991; Sommer-Larsen et al. 1999).

An alternative solution to the angular momentum distribution problem is that the feedback driven outflows preferentially discard low angular momentum material during the assembly of the galaxy (Brook et al. 2011b). In fact recent high resolution simulations including star formation and feedback have been quite successful in forming bulge-less exponential discs (Governato et al. 2010; Brook et al. 2011b) where such a process has been shown to occur. Understanding the spatial distribution of the low angular momentum material might shed light as to which method might be more effective in solving the angular momentum distribution problem.

According to the model proposed by Maller & Dekel (2002), the most favorable scenario for galaxy formation is, where there are very few minor mergers, e.g., a halo acquiring its angular momentum via a major merger. Is it enough to generate angular momentum distributions such that exponential discs can be formed? If the gas distribution is concentrated due to cooling or puffed up as with feedback, does it change the angular momentum distribution of merger remnants? These are some of the questions that we investigate.

The angular momentum properties of galaxies is of increasing interest in observational surveys. New imaging fibre bundles (so called hexabundles) are to be used on wide-field survey telescopes (e.g., AAT; Bland-Hawthorn et al. 2011; Bryant et al. 2011) to obtain spatially resolved stellar and gas kinematics for a volume-limited sample 10^{4-5} galaxies. It will then be possible to study the angular momentum distribution of galaxies in voids, filaments, groups and clusters. Although current simulations which include star formation and feedback have started showing success in forming disc galaxies, but these simulations are computationally very expensive and this prohibits generation of a large sample of galaxies for statistical studies. On the other hand dark matter only simulations are computationally much less demanding which makes them suitable for comparison with large scale galaxy surveys, but one needs a way to populate dark matter halos with galaxies. Semi-analytic modelling of galaxies provides a way to do this (Cole et al. 1994; Baugh et al. 1996; Kauffmann et al. 1999; Somerville & Primack 1999; Kauffmann & Haehnelt 2000; Benson et al. 2003; Kang et al. 2005), but a crucial assumption that is often made is that the angular momentum properties of gas is same as that of dark matter. This provides another motivation for studying the differences between the angular momentum properties of gas and dark matter. A few example applications where such a difference could play an important role are discussed below.

The spin parameter plays a crucial role in governing the properties of the galaxies. The spin of dark matter halos has been extensively studied. and it has been shown that the distribution is well fit by a log normal distribution (Bett et al. 2010, 2007; Sharma & Steinmetz 2005; van den Bosch et al. 2002; Neto et al. 2007; Macciò et al. 2007). In Sharma & Steinmetz (2005) and Chen et al. (2003), it was also found that for halos simulated in cosmological context, the gas in general has higher spin parameter than that of dark matter. Additionally, Sharma & Steinmetz (2005) found the ratio to increase at lower redshifts with a value of $\lambda_{\rm gas}/\lambda_{\rm DM} \sim 1.4$ at redshift zero. The cause of this is still not known. Note, both Sharma & Steinmetz (2005) and Chen et al. (2003) found the spin parameter and shape parameter of AMDs to be higher for gas as compared to dark matter whereas van den Bosch et al. (2002) find the properties of gas and dark matter to be similar. This is probably due to the inclusion of a large number of halos with low particle numbers in the analysis of van den Bosch et al. (2002). Moreover, van den Bosch et al. (2002) had used thermally broadened gas velocities to compare the AMDs with that of dark matter, as shown in Sharma & Steinmetz (2005) this broadening of velocities masks out the differences in AMDs. Finally, van den Bosch et al. (2002) had analyzed the results at $z = 3$ whereas the other authors had analyzed them at $z = 0$.

Recently, it has been reported that high spin halos are more clustered than low spin halos (Bett et al. 2007; Davis & Natarajan 2010). Macciò et al. (2007) on the other hand do not find any environmental dependence. A crucial difference in the two schemes is the treatment of unrelaxed halos. It has been shown that out-of-equilibrium halos tend to have higher spin and low concentration, which when removed makes the halo concentration independent of spin (Gardner 2001; Vitvitska et al. 2002; Peirani et al. 2004; Hetznecker & Burkert 2006; Neto et al. 2007). Such an effect could also be responsible for higher clustering of high spin halos. D'Onghia & Navarro (2007) have studied the correlation of merger history and spin of halos and found that halos immediately after merger have higher spin. Later on during the virialization process the halos spin down due to redistribution of mass and angular momentum. Generally the offset of the center of mass is used to parameterize the unrelaxed halos. How effective is this parameter in detecting unrelaxed halos? Observationally it is the spin of the baryonic component that is observed, hence it is important to know if the gas also undergoes such a spin up and spin down during mergers?

Another area where gas shows a difference from dark matter is the issue of misalignment between them. The angular momentum of gas in galactic halos is found to be misaligned with respect to dark matter with a mean angle of 20° (Sharma & Steinmetz 2005; van den Bosch et al. 2002). The misalignment has important observational consequences. For example it has been found that the distribution of satellite galaxies is preferentially aligned along the major axis of the central galaxy (Brainerd 2005; Yang et al. 2006; Azzaro et al. 2007; Wang et al. 2008). Agustsson & Brainerd (2006) show that if the disc angular momentum vectors are aligned with the minor axis of the halo or the angular momentum of the halo then the observed anisotropy can be reproduced. Kang et al. (2007) further showed the second option is preferred as orientation with minor axis results in a stronger signal than that observed. If the angular momentum of gas is misaligned with the dark matter then this could potentially lower the signal. Another example is related to the use of weak lensing studies to measure the projected mass density of a foreground galaxy in front of background galaxies. Since signal from an individual galaxy is weak, to produce detectable signals, results of different galaxies are stacked together by orienting the images with respect to the shape of the central galaxy. If the angular momentum of the galaxies is misaligned with respect to the shape of the dark matter halos, then this can wash out any ellipticity signal in the projected mass distributions (Bett et al. 2010).

The angular momentum vectors of gas and dark matter, in addition to being misaligned with each other, are also not perfectly aligned with themselves within the halo (Bailin & Steinmetz 2005; Bett et al. 2010), which we refer to as self-misalignment. The self-misalignment is found to be most pronounced between the inner and outer parts (Bailin & Steinmetz 2005). For the gas such a self misalignment could be responsible for warps as seen in galactic discs. In recent cosmological hydrodynamical simulations, Roškar et al. (2010) show that the warps in their discs are due to the misalignment of the angular momentum of the inner cold gas with that of the outer hot gaseous halo. Hence, it is important to understand as to when such a misalignment occurs.

The self misalignment of angular momentum could also be responsible for the counter rotating gas as seen in some of the galaxies (Ciri et al. 1995; Sil'chenko et al. 2009; Sil'chenko & Moiseev 2006). Although, recent mergers of gas rich systems are generally used to explain them, but they have some shortcomings. For example, if the merger is too massive it can heat up and thicken the disc considerably; if it is small then in some cases it cannot account for all of the counter rotating gas (Thakar & Ryden 1996; Ciri et al. 1995). Misaligned angular momentum in galactic halos could provide an explanation for this.

To answer some of the questions posed earlier, we perform hydrodynamical simulations of merging spherical halos and analyze the angular momentum distributions of the resulting remnant halos. We do simulations with various different orbital parameters and study the dependence of the shape parameter α of angular momentum distributions on these orbital parameters. We also analyze the ratio $\lambda_{\rm gas}/\lambda_{\rm DM}$ and the misalignment angle θ of the remnant halos.

After a brief discussion of parameters related to merger in Section 2, we describe details of setting up initial conditions and methods of extracting angular momentum distributions from halos in Section 3. In Section 4 we analyze the mass structure of remnant halos and then in Section 5 we investigate the angular momentum properties of these halos. Finally, in Section 6 we summarize and discuss our results.

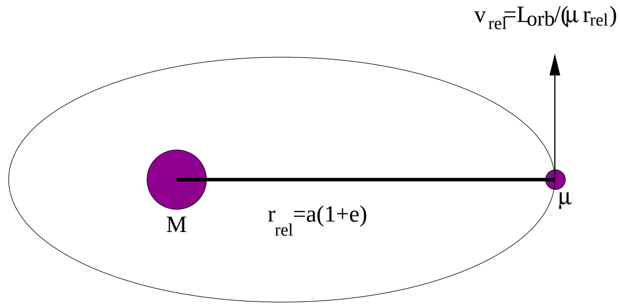

FIG. 1.— Merger of two halos can be reduced to a one body problem of mass μ moving in the potential of mass M. The orbit can be characterized by semi-major axis a and eccentricity e. At maximum separation $r_{\rm rel} = a(1+e)$ the tangential velocity $v_{\rm rel}$ is given by the angular momentum acquired by the masses during the expansion phase.

2. ORBITAL PARAMETERS

The merger of two bodies of mass m_1 and m_2 can be reduced to the motion of a test particle, with a reduced mass $\mu = m_1 m_2/(m_1+m_2)$, in the potential of a mass $M = m_1 + m_2$ (Figure 1). The initial conditions are set by specifying the relative separation $\mathbf{r}_{\rm rel}$ and relative velocity $\mathbf{v}_{\rm rel}$. In a cosmological context the two masses first move apart due to Hubble expansion and eventually, come to a halt and collapse due to their mutual gravitational attraction. The orbits of interest are those which are bound and collide within a Hubble time. A bound orbit can be fully characterized by its eccentricity e and the semi-major axis a. The energy of the orbit $E_{\rm orb}$, and the orbital time period $T_{\rm orb}$ are related to a by

$$E_{\rm orb} = -\frac{GM\mu}{2a} \quad , \quad T_{\rm orb} = 2\pi\sqrt{\frac{a^3}{GM}} \tag{1}$$

$E_{\rm orb}$ can be written in terms of $T_{\rm orb}$ as

$$E_{\rm orb} = -\frac{1}{2}(4\pi^2 G^2)^{1/3} T_{\rm orb}^{-2/3} f_\mu M^{5/3} \tag{2}$$

where $f_\mu = \frac{\mu}{M}$. The angular momentum $L_{\rm orb}$ is related to eccentricity e by

$$L_{\rm orb} = \mu\sqrt{GMa}\sqrt{1-e^2} \tag{3}$$

$$= \frac{GM^{5/2} f_\mu^{3/2}\sqrt{1-e^2}}{\sqrt{2|E_{\rm orb}|}} \tag{4}$$

According to the tidal torque theory the system acquires angular momentum during its expansion phase, with the angular momentum increasing nearly linearly with time during the initial linear phase of growth of density perturbations (White 1984). The acquisition of angular momentum ceases in the non-linear regime. We assume that all angular momentum is acquired by the time of maximum expansion which gives

$$r_{\rm rel} = a(1+e) \tag{5}$$

At maximum expansion, the radial velocity being zero, the total velocity is given by the tangential velocity.

$$v_{\rm rel} = \frac{L_{\rm orb}}{\mu r_{\rm rel}} \tag{6}$$

Since the merging bodies are extended objects, the total energy is given by the sum of the orbital energy plus the self energy of the bodies. The self energy of a body of mass M_v and radius R_v, having an NFW density profile (Navarro et al.

1996, 1997) with concentration parameter c, is given by [1]

$$E_v = -f_c \frac{GM_v^2}{2R_v} \quad (7)$$

$$\text{where} \quad f_c = \frac{c}{2}\frac{1 - 1/(1+c)^2 - 2\ln(1+c)/(1+c)}{(\ln(1+c) - c/(1+c))^2} \quad (8)$$

Assuming that both halos are virialized at a redshift of z, M_v can be written in terms of R_v are as

$$M_v = \frac{4\pi R_v^3}{3}\Delta(z)\Omega_m \frac{3H^2(z)}{8\pi G} \quad (9)$$

$$= R_v^3 \frac{\Delta(z)\Omega_m H^2(z)}{2G}, \quad (10)$$

where $\Delta(z)$ is the over-density criteria used to identify a virialized region, i.e., a spherical region whose average mass density is $\Delta(z)$ times the mean matter density at that redshift. $\Delta(z)$ is approximated by (Bryan & Norman 1998) $\Delta(z) \simeq (18\pi^2 + 82x + -39x^2)/(1+x)$, where $x = \Omega_m(z) - 1$.

Consequently, the total energy is given by

$$E = E_{v1} + E_{v2} + E_{\rm orb} \quad (11)$$

Analogously, the spin parameter λ of the whole system is given by

$$\lambda = \frac{L|E|^{1/2}}{GM^{5/2}} \quad (12)$$

$$= \sqrt{\frac{1-e^2}{2}} f_\mu^{1.5} \left(\frac{|E|}{|E_{\rm orb}|}\right)^{1/2} \quad (13)$$

Instead of the semi-major axis a and the eccentricity e the orbit can be equivalently parameterized in terms of the orbital time period $T_{\rm orb}$ and the spin parameter λ. We restrict ourselves to values of $T_{\rm orb}$ which have $r_{\rm rel} > r_{12}$ where $r_{12} = r_{\rm vir1} + r_{\rm vir2}$.

3. METHODS

3.1. *Initial Conditions and Simulations*

We study binary mergers of spherical halos consisting of dark matter and gas. The halos are set up with an NFW density profile along with an exponential truncation.

$$\rho(r) = \begin{cases} \frac{\rho_s}{(r/r_s)(1+r/r_s)^2} & \text{for } r < r_{\rm vir} \\ \frac{\rho_s}{(r_{\rm vir}/r_s)(1+r_{\rm vir}/r_s)^2}\left(\frac{r}{r_{\rm vir}}\right)^\epsilon \exp(-\frac{r-r_{\rm vir}}{r_d}) & \text{for } r > r_{\rm vir} \end{cases} \quad (14)$$

Imposing the condition that the logarithmic slope of ρ at $r = r_{\rm vir}$ should be continuous, gives

$$\epsilon = r/r_{\rm vir} - \frac{1+3c}{1+c} \quad (15)$$

For all our set ups we use $r_d = 0.1 r_{\rm vir}$. The exponential truncation gives rise to an extra mass, which we compensate by truncating at $r < r_{\rm vir}$, such that the total mass of the system is $m_{\rm tot} = m_{\rm vir}$. For generating equilibrium realizations of the system, comprising of collisionless particles, we follow the procedure given by Kazantzidis et al. (2004). In this procedure, first the phase space distribution function corresponding to a given density profile is numerically evaluated and then the velocities of the collisionless particles are assigned by randomly sampling this distribution. The gas is setup in hydrostatic equilibrium within the dark matter halo assuming a density profile identical to that of the dark matter ($\rho_{\rm gas}(r) = \rho_{\rm DM}(r) f_b/(1-f_b)$, $f_b = \Omega_{\rm baryon}/\Omega_{\rm matter}$ being the cosmological baryon fraction). The thermal energy of the gas is given by

$$u(r) = \frac{1}{\rho_{\rm gas}(r)}\int_r^\infty \rho_{\rm gas}(r)\frac{GM(r)}{r^2}dr \quad (16)$$

where $M(r)$ is the cumulative total mass enclosed by radius r.

In Table 1 we list the parameters that are used to set up 11 simulations with $N = 2 \times 10^5$ dark matter particles and an equal number of gas particles. $T_{\rm orb}$ is chosen such that $r_{\rm rel} = r_{12}$ except for Sim 6, which was started with $r_{\rm sep} = r_{12}$ (see Section 2 for details). In Sim 1 to 8 we assume the density distribution of gas to be same as that of dark matter but in Sim 10 and 11 the gas is allowed to have a different density distribution, namely the concentration parameter for gas is different from that of dark matter and this is shown in brackets. All the simulations except Sim 9 start with non-rotating halos, i.e., zero intrinsic spin. For the Sim 9 we use the remnant halo obtained from Sim 1 as initial halo and $L_{\rm orb}$ is set to be perpendicular to the spin L_{int} of the halos. The intrinsic halo spins are assumed to be parallel to each other and point towards the z axis. For this setup the direction of orbital angular momentum in spherical coordinates is given by $(\phi,\theta)_{\rm orb} = (-90, 90)^\circ$. Three other setups similar to this but with $(\phi,\theta)_{\rm orb} = (-90, 45)^\circ$, $(-90, 135)^\circ$ and $(-90, 180)^\circ$ were also performed but are not listed in Table 1.

All simulations were evolved for 10 h^{-1} Gyr. The simulations were done using the smooth particle hydrodynamics code GADGET (Springel et al. 2001). By construction, no assumptions on a particular background cosmology are made; however, for the NFW halo parameters we adopt the concordance ΛCDM cosmology with $\Omega_\lambda = 0.7$, $\Omega_m = 0.3$.

In order to compare the angular momentum properties of merger simulations with those of simulations done in cosmological context we additionally use a set of 42 halos (virial masses between $1.3 \times 10^{11} M_\odot$ to $1.5 \times 10^{13} M_\odot$), which were selected from a 32.5 $\mathrm{h}^{-1} Mpc$ box length dark matter simulation (128^3 particles), and were resimulated with gas at higher resolution by Sharma & Steinmetz (2005) using GADGET. In these halos the number of dark matter particles within the virial radius ranges from 8000 to 80,000.

3.2. *Calculation of angular momentum distributions*

Dark matter particles are assumed to be collisionless and thus a significant amount of random motions are superimposed onto the underlying rotational motion. So in order to calculate angular momentum distributions, the velocity has to be smoothed (see Sharma & Steinmetz 2005). Since the rotational motion is very small compared to the random motion, one needs to smooth with a large number of neighbors. This large scale smoothing introduces systematic biases which needs to be taken into account. Smoothing the Cartesian components of velocity spuriously underestimates the rotation for particles near the axis, as $< v_x > = < v_y > = < v_y > \approx 0$ near the axis. To avoid this problem in Sharma & Steinmetz (2005) we smoothed the Cartesian components of angular momentum vectors instead of velocities. As we will demonstrate later, the angular velocity Ω is nearly constant near the center.

[1] For the Einasto profile the formulas are available at Nichols & Bland-Hawthorn (2009, 2011)

TABLE 1
ORBITAL PARAMETERS: λ' IS THE FINAL SPIN PARAMETER OF THE VIRIALIZED REMNANT HALO AT $t = 10\,\mathrm{h}^{-1}$ Gyr. IT IS CALCULATED USING THE DEFINITION $\lambda' = \mathrm{J}_{\rm total}/(\sqrt{2}R_{\rm vir}V_{\rm vir})$ (BULLOCK ET AL. 2001), WHERE $\mathrm{J}_{\rm total}$ IS THE SPECIFIC ANGULAR MOMENTUM OF A HALO HAVING VIRIAL RADIUS $R_{\rm vir}$ AND VIRIAL VELOCITY $V_{\rm vir} = \sqrt{GM_{\rm vir}/R_{\rm vir}}$. $f_m = \frac{m_2}{(m_1+m_2)}$ IS THE FRACTIONAL MASS OF THE LEAST MASSIVE HALO.

Sim	$M_{\rm tot}$ 10^{10} h^{-1} $\mathrm{M}_\odot$	f_m	$\lambda_{\rm orb}$	$c_{\rm initial}$	$T_{\rm orb}$ h^{-1} Gyr	λ_{int}	$M_{\rm vir}$ 10^{10} h^{-1} $\mathrm{M}_\odot$	f_b	$c_{\rm final}$	θ	$\lambda'_{\rm gas}$	$\lambda'_{\rm DM}$	$\lambda'_{\rm gas}/\lambda'_{\rm DM}$		$\alpha_{\rm DM}$	$\alpha_{\rm gas}$	$f_{\rm neg}$
1	100	0.5	0.05	10.0	6.70	0.0	83.6	1.0	10.4	0.4	0.037	0.039	0.96(1.17)	0.87	0.85	0.97	0.03
2	100	0.5	0.05	5.0	6.70	0.0	83.4	1.02	5.75	0.6	0.042	0.039	1.08(1.27)	0.94	0.87	1.08	0.02
3	100	0.5	0.05	15.0	6.68	0.0	84.4	1.0	15.1	0.8	0.035	0.038	0.91(1.10)	0.84	0.78	0.90	0.05
4	100	0.5	0.01	10.0	6.40	0.0	84.2	1.0	10.8	1.7	0.0079	0.0084	0.94 (1.04)	0.81	0.89	0.93	0.21
5	100	0.5	0.10	10.0	7.50	0.0	83.3	1.03	11.3	0.4	0.093	0.074	1.25 (1.30)	1.0	0.86	1.02	0.003
6	100	0.5	0.05	10.0	10.0	0.0	80.2	1.02	10.5	0.1	0.043	0.037	1.15(1.49)	0.92	0.79	0.96	0.02
7	100	0.1	0.05	10.0	7.40	0.0	91.8	0.95	9.2	2.0	0.046	0.024	1.96(1.62)	1.3	0.82	0.74	0.12
8	100	0.3	0.05	10.0	6.60	0.0	86.6	0.99	10.5	1.2	0.044	0.037	1.17(1.28)	0.95	0.85	0.86	0.10
9	167.2	0.5	0.05	10.08	6.70	0.039	137.5	1.04	11.5	18.2	0.044	0.041	1.09(1.22)	0.82	0.75	0.94	0.08
10	100	0.5	0.05	10(1)	6.70	0.0	79.3	0.80	8.9	2.2	0.029	0.036	0.79(0.68)	0.88	0.82	1.02	0.13
11	100	0.5	0.05	10(25)	6.70	0.0	84.5	1.06	14.3	1.5	0.036	0.041	0.88(0.94)	0.74	0.81	0.91	0.12

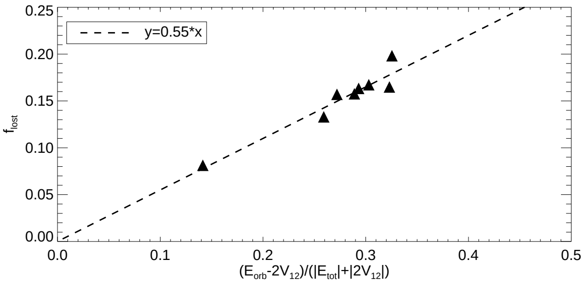

FIG. 2.— Dependence of fraction of mass lost during a collision on merger parameters. The fraction of mass lost is an increasing function of the kinetic energy involved in the collision and a decreasing function of the total binding energy of the system.

This implies that the angular momentum (hereafter AM) vector j has a strong, monotonically increasing radial dependence on cylindrical co-ordinate r_c. This results in an overestimate of the AM of particles close to the axis. Existence of a strong radial density gradient further leads to underestimate of AM for particles along the equator. To reduce some of these problems, in this paper we choose to smooth the angular velocity vector $\mathbf{\Omega}$. A simple top hat kernel is used for smoothing. For a halo with approximately 2×10^5 particles we use 400 neighbors for smoothing and scale it linearly for a halo with larger number of particles. Smoothing is only employed to calculate the shape parameter α of the resulting angular momentum distributions.

4. MASS STRUCTURE OF REMNANT HALOS

The final properties of the merger remnants are given in Table 1. We note that the virial mass $M_{\rm vir}$ of the remnant is less than the total mass of the system $M_{\rm tot}$. Hence, a fraction of mass is lost which we define as $f_{\rm lost} = (M_{\rm tot} - M_{\rm vir})/M_{\rm tot}$. Also, the concentration parameter of the remnant halo $c_{\rm final}$ is slightly larger than $c_{\rm initial}$.

It is interesting to know if the final properties of the halo e.g., $M_{\rm vir}$ and $c_{\rm final}$ can be predicted from the initial conditions. We expect the fraction of lost mass $f_{\rm lost}$ to be an increasing function of the kinetic energy KE involved in the collision and a decreasing function of the total binding energy of the system. We find that the following empirical formula, which satisfies the above conditions, fits the results obtained from simulations (Figure 2).

$$f_{\rm lost} \propto \frac{\text{Maximum KE of collision at } r_{\rm sep} = r_{12}/2}{|E_{\rm tot}| + \text{PE at } r_{\rm sep} = r_{12}/2} \quad (17)$$

$$= k_f \frac{E_{\rm orb} - 2V_{12}}{|E_{\rm tot}| + |2V_{12}|} \quad \text{where } V_{12} = -\frac{GM\mu}{r_{12}} \quad (18)$$

If $c_{\rm initial}$ is higher the system has higher $|E_{\rm tot}|$ consequently, it is more bound and loses less mass. If $|E_{\rm orb}|$ is higher the system is again more bound and also the KE of the collision is less, consequently reducing the mass loss.

Interestingly, the total energy of the remnant halo $E_{\rm vir}$ (putting $c_{\rm final}$ and $M_{\rm vir}$ from Table 1 in Equation (7)) is nearly equal to the energy of the system $E_{\rm total}$ before the merger. This suggests that the mass that lies outside the virial radius, consists of a bound and an unbound part and has almost zero net energy. Consequently the concentration parameter of a remnant halo can be predicted from the knowledge of its orbital parameters.

5. ANGULAR MOMENTUM STRUCTURE OF REMNANT HALOS

5.1. *Angular velocity and angular momentum distribution of halos*

We first explore the angular velocity Ω as function of spherical co-ordinates r and θ for the remnant halos at $t = 10\,\mathrm{h}^{-1}$ Gyr, which represents the final relaxed configuration. The angular velocity Ω of both gas and dark matter is found to be nearly independent of θ, both for $r < r_{\rm vir}$ and $r < r_{\rm vir}/2$ (lower two panels of Figure 3). This suggests that shells of matter are in solid body rotation. The top panel in Figure 3 shows the radial profiles of gas and dark matter. In general Ω is a decreasing function of radius r but the profiles seem to flatten for $r < 0.2r_{\rm vir}$. As compared to dark matter, the gas is found to rotate faster in the inner regions and slower in the outer regions. For comparison the angular velocity profiles of halos simulated in cosmological simulations (from Sharma & Steinmetz (2005)) are shown in Figure 4. As in merger simulations they are also nearly independent of angle θ, are a decreasing function of radius r, and show faster rotation for gas in the inner regions. However, the faster rotation for gas is not as strong as in merger simulations and the dip in gas rotation at about $r = 0.7r_{\rm vir}$ is also not seen. Note, these are median profiles, on a one to one basis the gas and dark

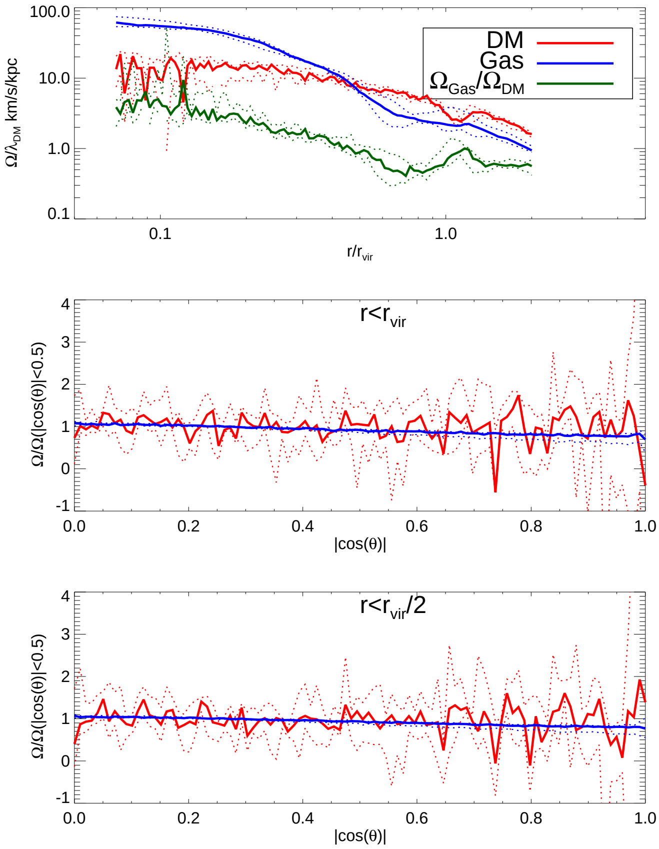

FIG. 3.— Median angular velocity $\Omega = j_z/(x^2+y^2)$ as function of radius r and angle θ for halos formed by mergers (merger simulations 1 to 8, excluding 4). Ω as a function of r and θ was calculated by binning the particles so as to 1000 particles per bin. The dashed lines show 16th and 84th percentile values. The angular velocity profiles seems to flatten out for $r < 0.2r/r_{\rm vir}$. In the top panel it can be seen that in the inner regions the gas rotates faster than dark matter. Note, the gas profiles are much more smooth than that of dark matter and this is because the dark matter has significant amount of random motion superimposed on the actual rotation which is quite small.

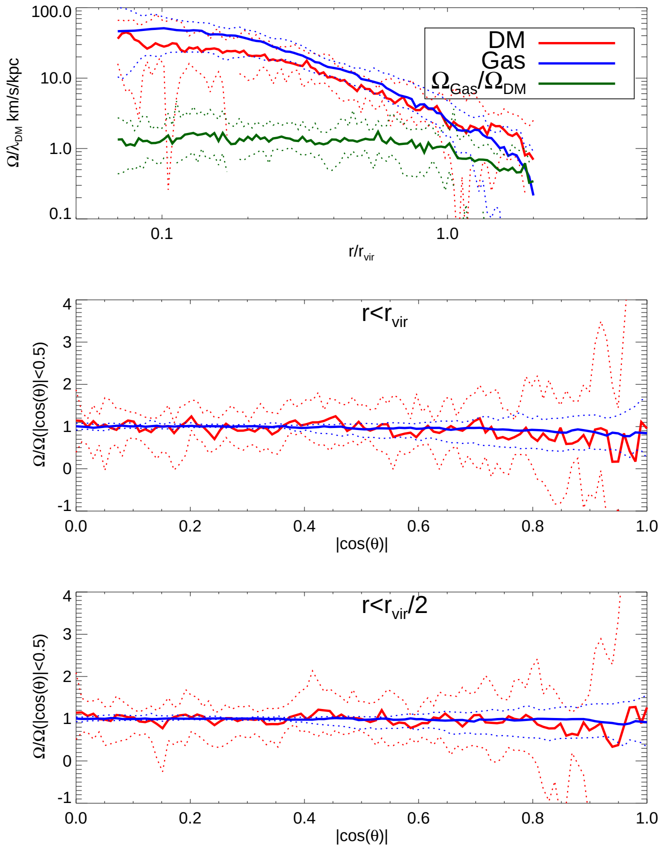

FIG. 4.— Median angular velocity $\Omega = j_z/(x^2+y^2)$ as function of radius r and angle θ for 21 halos simulated in a cosmological context. The halos where selected so as to have more than 30,000 particles within the virial radius individually for both gas and dark matter. Ω as a function of r and θ was calculated by binning the particles so as to have 1000 particles per bin. The dashed lines show 16th and 84th percentile values. The angular velocity profiles seems to flatten out for $r < 0.2r/r_{\rm vir}$. In the top panel it can be seen that the gas rotates faster in the inner regions than that of dark matter.

matter can show much more prominent differences as is revealed by the fact that there is significant scatter in the ratio $\Omega_{\rm gas}/\Omega_{\rm DM}$. Also a real halo has much more complex merger history which can probably reduce the difference between dark matter and gas in the inner regions. The difference in outer parts is probably due to the fact that the initial merging halos have an exponential cut off in outer parts whereas in real simulations the halos are much more extended and moreover there is also smooth accretion onto the halos. Hence outer parts of merger remnants might not be an accurate representation of the real halos.

We now study the angular momentum distributions (hereafter AMD) of the remnant halos at $t = 10\ {\rm h}^{-1}$ Gyr. The angular momentum of each particle is obtained by smoothing its angular velocity with 400 neighbors. For fitting the AMDs we use the following analytical function (for details see Sharma & Steinmetz 2005)

$$P(j) = \frac{1}{j_d^{\alpha}\Gamma(\alpha)}(j)^{\alpha-1}e^{-j/j_d}\text{where } j_d = j_{\rm tot}/\alpha. \quad (19)$$

$j_{\rm tot}$ being the total specific angular momentum of the system. Writing P in terms of $s = j/j_{\rm tot}$ and replacing j_d the cumulative distribution reads as

$$P(<s) = \gamma(\alpha, \alpha s) \quad (20)$$

where γ is the Incomplete Gamma function. In Sharma & Steinmetz (2005) this function was used to fit the AMDs of halos obtained in cosmological simulations and of model exponential disks embedded in NFW potentials. It was found that for AMDs of exponential disks embedded in NFW potentials the shape parameter α is greater than 1.3 whereas for cosmological halos values are typically smaller than 1 ($<\alpha_{\rm DM}>= 0.83$ and $<\alpha_{\rm gas}>= 0.89$). For dark matter for fiducial Sim 1 we find $\alpha = 1$ whereas for others it is given by $0.75 < \alpha < 0.9$. For gas for Sim 1 α is 0.97 and for others it is between 0.74 and 1.08. The gas has significantly larger α than dark matter and this is because of the fact that the gas rotates faster than dark matter in the inner regions. Merger simulations successfully reproduce the fact that $\alpha_{\rm gas} > \alpha_{\rm DM}$ as in cosmological simulations. If we take Sim 1 as the fiducial case then for dark matter the value of α is in excellent agreement with cosmological simulations but for gas we find that it is about 8% higher. As discussed earlier the gas in merger simulations are an idealized case and in real halos the gas rotation profiles are slightly flatter in the outer parts and this explains the slightly lower α in them.

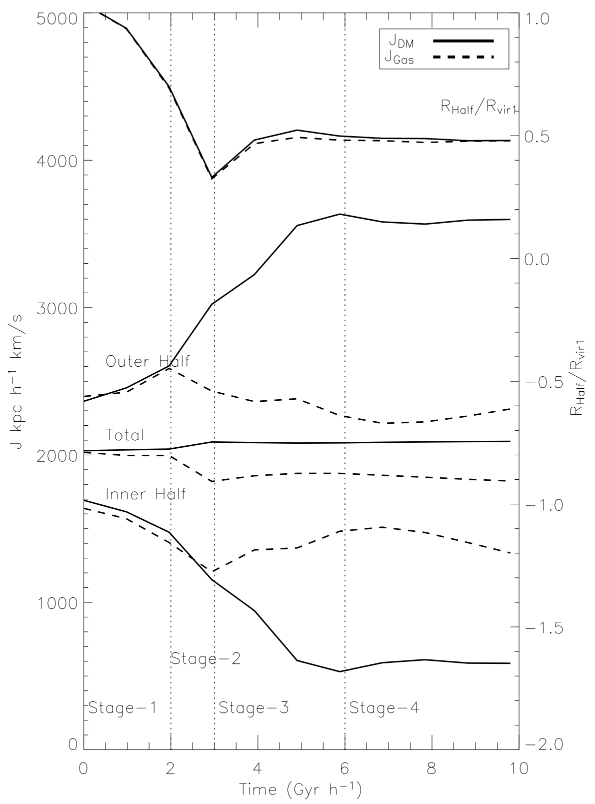

FIG. 5.— Evolution of specific angular momentum J of gas and dark matter components for Sim 1 (an equal mass merger). $R_{\rm half}$ which is the radius of a sphere containing half of the total mass of the corresponding component is also plotted alongside. $R_{\rm vir1}$ is the virial radius of the parent halo. Angular momentums for the inner half mass, and outer half mass are shown separately.

5.2. *Evolution of angular momentum with time*

In this section we analyze the time evolution of the specific angular momentum of gas and dark matter components for Sim 1 (Figure 5), which is an equal mass merger of halos with concentration parameter of 10, $T_{\rm orb} = 6.7\,{\rm h}^{-1}$ Gyr and $\lambda_{\rm initial} = 0.05$. We use this as a fiducial case to understand the main properties of the evolution, specifically the origin of the differences in the angular momentum properties of gas and dark matter. We analyze the evolution of the total angular momentum as well as that of the inner and the outer parts separately. For this we divide the halo into an inner and outer half by mass. The evolution of $R_{\rm half}$, the radius of a sphere containing half of the total mass of the system, is also plotted alongside. We divide the evolution into four stages, Stage 1 from $0 - 2\,{\rm h}^{-1}$ Gyr, Stage 2 from $2 - 3\,{\rm h}^{-1}$ Gyr, Stage 3 from $4 - 6\,{\rm h}^{-1}$ Gyr and Stage 4 from $6 - 10\,{\rm h}^{-1}$ Gyr.

During a merger the system first collapses to a compact configuration in Stage 1 and Stage 2, which is marked by a decrease in $R_{\rm half}$ (see also Figure 6). In Stage 3 the system expands, as shown by the slight increase in $R_{\rm half}$, and then in Stage 4 the system evolves without any significant change in the density structure. It can be seen from the evolution of the total AM of the system (middle lines in Figure 5) that in Stage 2 the gas loses about 10% of its AM to DM. The DM gains AM in this stage but its change is quite small since the mass of DM is much larger than that of gas. In Stage 3 and 4 the total AM of gas and DM is nearly constant. In contrast, when the AM of inner and outer half masses are analyzed separately, significant differences can be seen. For DM there is an inside out transfer of AM in stages 1, 2 and 3. Due to dynamical friction the inner part loses AM continuously to the outer part until it virializes to form a pseudo equilibrium distribution after which the evolution stops. It can be seen that the AM evolution of gas is decoupled from DM, from stage 2 onwards. Initially, both the inner and outer parts of gas lose angular momentum to DM. However, in Stage 3, when the inner parts start to expand, for the gas the AM is transferred to the inner parts from the outer parts. The fact that the rise in AM of gas in inner parts is almost same as the fall in AM of gas in outer parts means that the transfer of AM is purely between the gas components. This transfer is because the expanding inner part of gas that also has low AM, shocks with in-falling outer part that has high AM, thereby leading to transfer of AM. This is visible more clearly in Figure 6 where we plot the velocity field in the X-Y plane within a radius of $125\,{\rm kpc}$ and $|z| < 20$. At 3.0 Gyr the halos can be seen crossing each other and at 3.2 Gyr they have crossed and are now pushing against the outer material of the other halo which is still falling in. The outer material falling in from upper right and lower left corners pushes and transfers AM to the expanding inner regions. With time the shocks progressively move outwards.

In contrast the dark matter cannot shock, their particles can cross each other and they exchange energy and AM via violent relaxation. It is easier to understand their evolution in terms of an inside out spherical collapse simulation in which the inner regions collapse faster than the outer regions. In such a system as described in Binney & Tremaine (2008) a high energy particle in outer region falls into a gradually steepening potential and hence gains kinetic energy. Later when it starts to move out the inner region has already expanded and hence it has to climb out of a shallower potential. The net result of all this is that a high energy particle that falls in late gains energy. Now, the impact parameter of the particle during collision is high for particles in the outskirts that are falling in late. Since the angular momentum of a particle is proportional to the impact parameter it is also high for them. Hence, high AM particles mostly end up orbiting in the outer regions. In contrast for gas these late falling high AM material shocks and transfers its AM to the inner parts.

Overall the conclusion is that due to gas dynamical effects the baryons are more efficient in depositing the AM to the inner parts of the halo and this results in different radial profiles of angular velocity as seen in Figure 3. The faster rotation of the gas in the inner region is also visible in the bottom panels of Figure 6.

This suggests that increasing the energy of the collision should make the outside-in transfer of AM for gas and inside-out transfer of AM for dark matter more stronger. The Sim 6 which is same as Sim 1 except for the fact that it has higher $T_{\rm orb}$ meaning more energetic merger does reveal this. It has lower $\lambda_{\rm DM}$ and higher $\lambda_{\rm gas}$ as compared to Sim 1 thus providing support to the above hypothesis.

In the final Stage 4 of the evolution the system has almost reached a pseudo equilibrium. During this stage, for the gas there is a gradual transfer of AM from the fast rotating inner layers to the slow rotating outer layers.

5.3. *Dependence of spin ratio $\lambda_{\rm gas}/\lambda_{\rm DM}$ on orbital parameters and its evolution with time*

Having understood the AM evolution in the inner and outer parts, we now try to understand the evolution of AM within

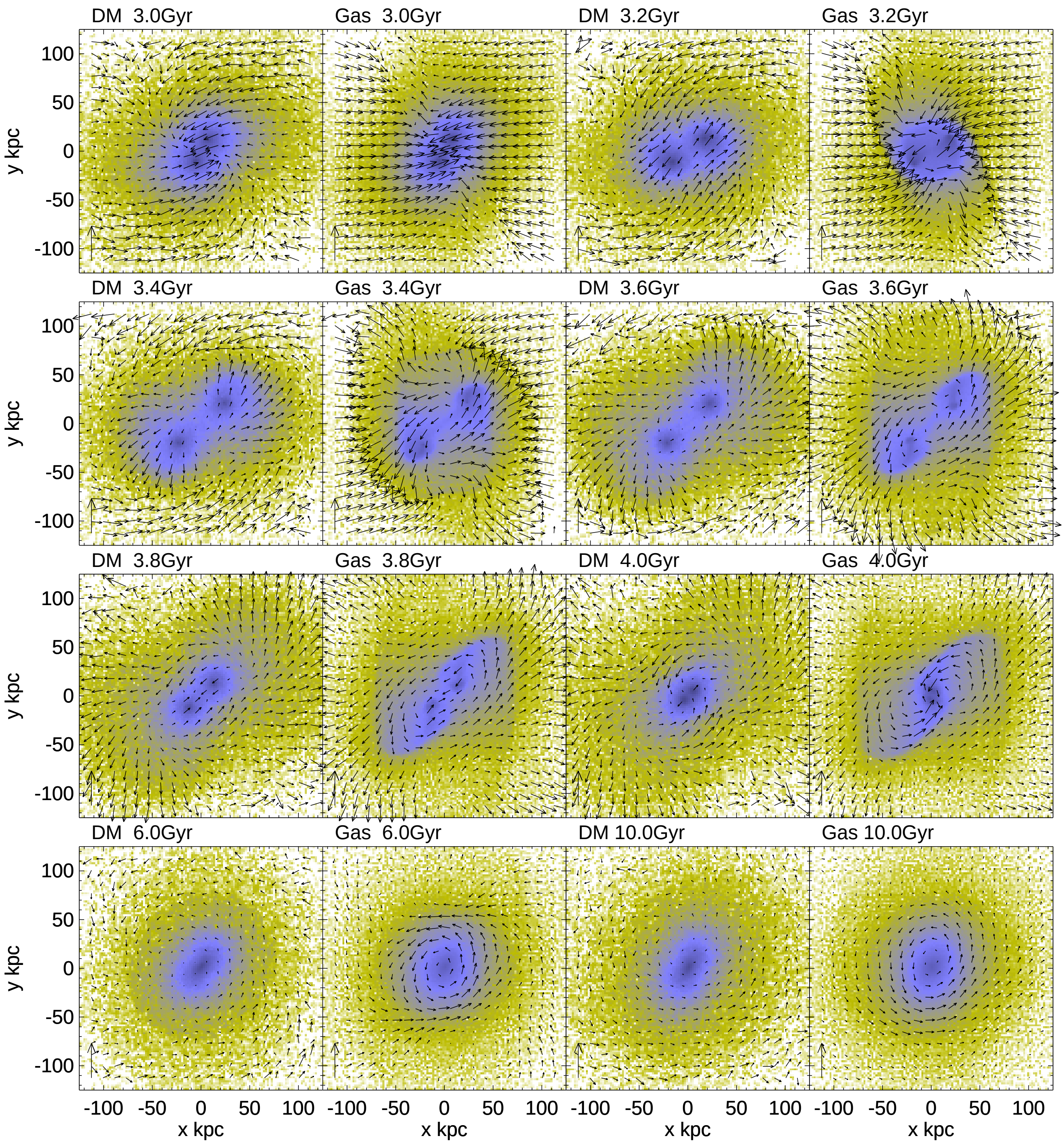

FIG. 6.— Velocity vector field in the X-Y plane along with density map for gas and dark matter at various stages during the evolution of an equal mass merger simulation (Sim 1). Field is shown for particles within a radius of 125 kpc and $|z| < 20$. The maximum length of the arrow corresponds to 250 kms and is shown in left hand corner of each panel. At 3.2 and 3.4 Gyr it can be seen that at the regions near the shocks (top right and lower left) the in-falling gas in the outer parts is transferring angular momentum to the inner parts. By $t = 6$ Gyr the gas can be seen to rotate faster in the inner regions as compared to dark matter.

the virial radius, which is commonly employed to measure the spin of the halos. Figure 7 describes the evolution of the spin ratio $\lambda_{\rm gas}/\lambda_{\rm DM}$ with time for various different merging scenarios. At each stage of the evolution we identify the virial region by means of the spherical over-density criterion and then compute the relevant properties of the virialized remnant halo. In Stage 1 ($0-2$ $\rm h^{-1}$ Gyr) of the evolution the ratio is close to 1. In Stage 2 ($2-3$ $\rm h^{-1}$ Gyr) the ratio drops by about $10-20\%$. In Stage 3 ($3-6\,\rm h^{-1}$ Gyr), the ratio rises and reaches a peak at around $6-7\,\rm h^{-1}$ Gyr and then in Stage 4 the ratio decreases (except for Sim 7). It is easy to understand the time evolution of spin ratios in the context of the discussion done earlier in Section 5.2. In Stage 1 the gas and dark matter have not yet decoupled so the ratio is close to 1. In Stage 2 the gas loses its angular momentum to DM and hence a drop in the spin ratio. In Stage 3, in the inner regions the dark matter loses AM while the gas gains, this results in a rise in the spin ratio. Finally, in Stage 4 the AM of dark matter in the inner

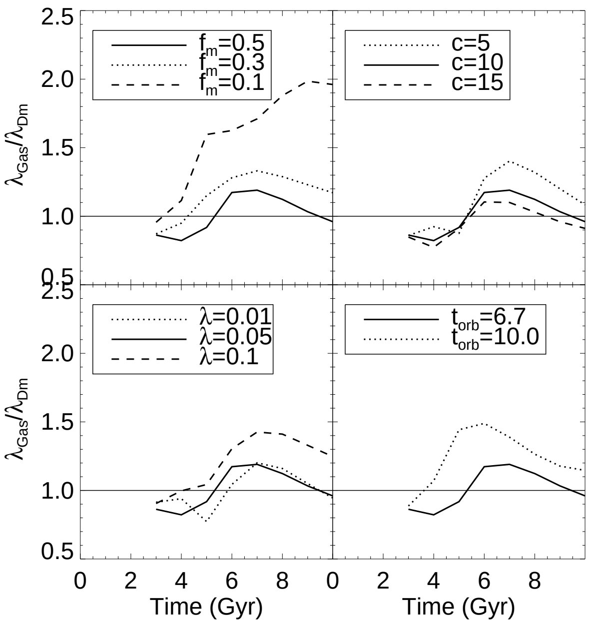

FIG. 7.— Evolution of $\lambda_{\rm gas}/\lambda_{\rm DM}$ with time for various merging scenarios.

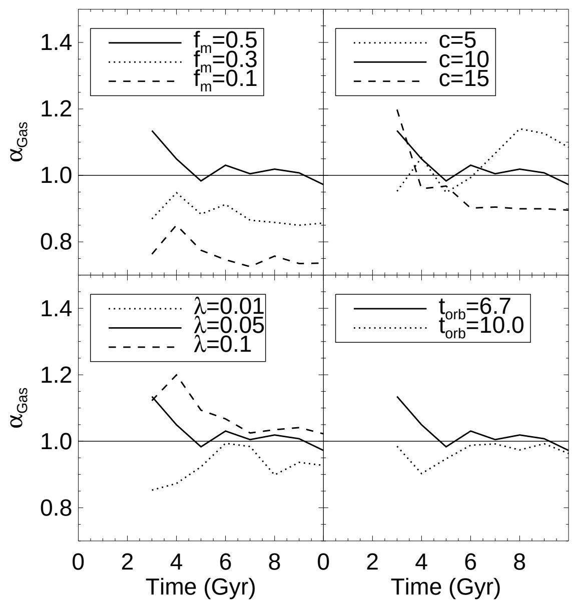

FIG. 8.— Evolution of $\alpha_{\rm gas}$ with time for various merging scenarios. α is calculated from the angular momentum distributions obtained from smoothing the motion of particles obtained from simulations.

regions remains nearly constant whereas for gas there is an inside out transfer and this again results in a drop in the spin ratio.

Next, we study the dependence of spin ratio on the orbital parameters. In each of the panels in Figure 7, we vary one of the orbital parameters (namely f_m, c, λ and $T_{\rm orb}$) while keeping the other parameters identical to that of benchmark Sim 1. In top left panel we compare Sim 1, 8 and 7, having f_m =0.5, 0.3 and 0.1 respectively, $f_m = m_2/M$ being the mass fraction of the smaller merging halo. At a given time the gas to dark matter spin ratio is found to be higher for a lower value of f_m. For $f_m = 0.1$ it continues to increase even in Stage 4 and reaches a value as high as 2.

In the second panel, i.e., top right, we plot the results for mergers with different values of concentration parameter, Sim 1, 2 and 3 having $c_{\rm initial}$ =10.0, 5.0 and 15.0 respectively. Lower concentrations yield higher spin ratios. It can be seen from Table 1 that $\lambda_{\rm DM}$ is largely unaffected by the change in $c_{\rm initial}$ whereas $\lambda_{\rm gas}$ increases with lowering the concentration. In Sim 10 and 11 we vary the concentration parameter of gas, setting it to 1 and 25 respectively, and keep the concentration of dark matter constant at 10.0. The Sim 10 is designed to mimic the case of a halo where the gas is puffed up by feedback from star formation whereas Sim 11 mimics the case where the gas has cooled and collapsed to the central regions. Table 1 shows that when considering the total angular momentum content, the concentrated gas loses more angular momentum than the puffed gas. This demonstrates the angular momentum catastrophe problem in which due to excessive cooling the gas gets concentrated and during subsequent evolution lose angular momentum as a result of dynamical friction. Surprisingly, when angular momentum is measured with in the virial region the puffed up gas has less angular momentum. This is because for the puffed up case significant amount of gas is outside the virial radius and this gas also has high angular momentum whereas for the concentrated gas case all the gas ends up within the virial radius. This is reflected in the baryon fraction as shown in Table 1 which is 0.8 for the former and 1.06 for the later.

In the bottom left panel we look at the role of varying the orbital angular momentum. We compare Sim 1, 4 and 5 having a $\lambda_{\rm orb}$ =0.05, 0.01 and 0.10 respectively. Increasing $\lambda_{\rm orb}$ beyond 0.05 increases the spin ratio while lowering it does not affect the results significantly. Finally, we investigate the role played by the kinetic energy associated with the collision, which is controlled by varying the parameter $T_{\rm orb}$. Larger $T_{\rm orb}$ means that halos approach each other from a farther distance and have more energetic collision. We compare Sim 1 and 6 which have $T_{\rm orb} = 6.7$ and 10.0 respectively. More energetic collisions lead to higher spin ratios. $\lambda_{\rm gas}$ increases as a result of increasing the impact velocity whereas the opposite is true for $\lambda_{\rm DM}$. In light of discussion in Section 5.2 this is because late infalling gas shocks more strongly leading to more transfer of AM to inner parts and for DM the late infalling gas is more energetic and is more likely to escape outside the virial radius.

In general it can be seen that at around 6 $\rm h^{-1}$ Gyr i.e., 3 $\rm h^{-1}$ Gyr after the merger the ratio $\lambda_{\rm gas}/\lambda_{\rm DM} > 1$ for all merging scenarios and this provides an explanation for the results of Sharma & Steinmetz (2005) and Chen et al. (2003) where they find $\lambda_{\rm gas}/\lambda_{\rm DM} \sim 1.4$ and 1.2 respectively for halos simulated in a cosmological context.

5.4. *Dependence of shape parameter α on orbital parameters*

In this section we explore the role of the orbital parameters on the shape parameter α obtained by fitting the AMD of the remnant halos by Equation (20). In Figure 9 we plot the evolution of the shape parameter $\alpha_{\rm gas}$ for various merging scenarios. The comparisons done in various panels are the same as in Figure 7. The values of α below $t = 3\ \rm h^{-1}$ Gyr are not relevant for the study here since the merger has not yet happened. Between $3-5$ Gyr there is a slight variation where the halo is still relaxing, but beyond that for all orbital geometries α has very little evolution with time (Figure 9).

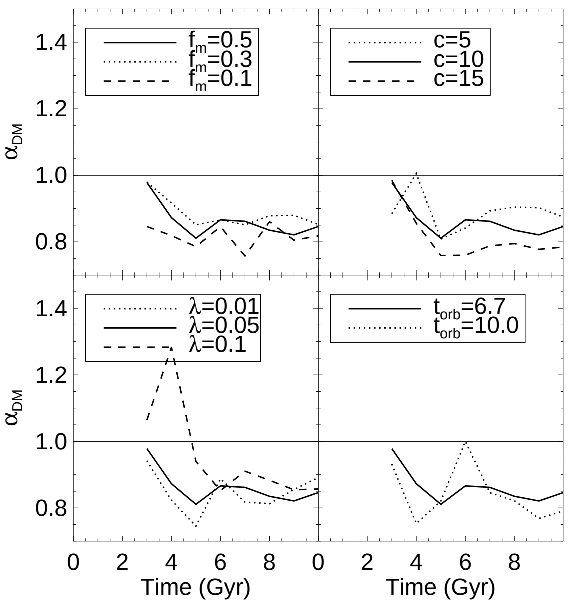

FIG. 9.— Evolution of $\alpha_{\rm DM}$ with time for various merging scenarios. α is calculated from the angular momentum distributions obtained from smoothing the motion of articles obtained from simulations.

As an apparent trend, α decreases slightly with time (except Sim 2). Varying the parameter $\lambda_{\rm orb}$ or $t_{\rm orb}$ does not seem to affect the values of α. Decreasing the mass ratio f_m decreases the value of α, while decreasing the concentration parameter $c_{\rm initial}$ increases its value. Varying only the concentration of gas as in Sim 10 and 11 also has similar effect (see Table 1), namely puffed up halos have higher α whereas concentrated halos have lower α. In the context of the angular momentum distribution problem this means puffing up gas by means of feedback does can partially help to resolve the problem, but the value of $\alpha = 1.02$ is still far short of that required to form exponential discs ($\alpha > 1.3$). Hence, just by itself the puffing up of gas is not enough to solve the problem.

Finally, we note that the gas in general has higher α than that of dark matter. This can also be seen in Table 1. This is again consistent with the findings of Sharma & Steinmetz (2005); Chen et al. (2003) for cosmological halos and provides a mean of explaining them.

5.5. *Misalignment of the AM vectors of gas and dark matter*

The misalignment angle θ for all simulations is tabulated in Table 1. Mergers with zero intrinsic spins do not seem to generate any significant misalignment in the final remnant halo. The misalignment angle θ is less than $2°$ for all orbital geometries. We have seen earlier that mergers with zero intrinsic spins give rise to halos which have $\rm J_{gas} > J_{DM}$ within the virial radius. Now if we imagine a merger of halos with non-zero intrinsic spins then in the final virial region $\mathbf{J}_{\rm gas}^{\rm intrinsic}$ could again be different from $\mathbf{J}_{\rm DM}^{\rm intrinsic}$ due to differences between the gas dynamics and collisionless dynamics. If $\mathbf{J}^{\rm intrinsic}$ is aligned with $\mathbf{J}^{\rm orbital}$ then again we do not expect to see any misalignment. However, if they are not in the same direction then final angular momentum of gas can point in a different direction than that of dark matter.

To test the above scenario, in Sim 9 we merge two halos (extracted from Sim 1) having non-zero spin and an orbital AM which is perpendicular to the spin. The remnant halo is found to be significantly misaligned with a misalignment angle close to $17°$. In Figure 10 we show the orientation of the angular momentum vectors of gas and dark matter as measured in radial shells for various different directions of the orbital angular momentum. We mainly concentrate on regions with $r > 0.1 r_{\rm vir}$ which should be quite reliable given that our gravitation softening is about $0.01 r_{\rm vir}$. The intrinsic spin has the direction $\theta = 0.0$. The solid and dashed lines are the differential profiles while the rest are cumulative profiles. In the top panel the lower horizontal line marks the mean expected θ for the halo assuming uniform mixing. The upper line shows the angle for the orbital AM. The gas and dark matter show very different trends. For DM the inner region is dominated by orbital AM, the outer by intrinsic spin and the middle region has intermediate direction. For the gas the inner region has intermediate values, the outer region is dominated by orbital angular momentum and the middle region is dominated by intrinsic spin, which points towards $\theta = 0°$. In the rightmost column corresponding to a retrograde merger the gas even shows a spin flip in the middle regions.

In the bottom panels it can be seen that the cumulative misalignment angle defined as $\beta_{\rm DM-gas}(<r) = \cos^{-1}(\hat{\mathbf{j}}_{\rm DM}(<r).\hat{\mathbf{j}}_{\rm DM}(<r))$ increases inwards into the halo. The cumulative self misalignment of the angular momentum, $\beta_{\rm DM-DM}$ and $\beta_{\rm gas-gas}$, which is measured with respect to the angular momentum with in the virial radius also shows similar trend. In the bottom row the magnitude of misalignment increases from left to right, i.e., with increase of angle between orbital and intrinsic AM.

In the panels in second column, the case of $\theta_{\rm orb} = 90$, it can be seen that most of the misalignment is due to the ϕ direction varying sharply in the inner regions. Moreover, the gas and and dark matter angular momentum vectors seem to be pointing in opposite directions in ϕ. This is surprising given the expected value of ϕ is $-90°$. It is not clear, if the gas is being torqued by dark matter or is it simply rearrangement of angular momentum. To understand this cumulative profiles are plotted as dotted lines. By $r = r_{\rm vir}$ the ϕ seems to have averaged to the expected value for both gas and dark matter. Also, in θ the cumulative profiles tend to the expected value at large r for both DM and gas. This suggests redistribution and self torquing to be the main mechanism for the variation of the direction gas angular momentum. However, beyond $r_{\rm vir}$, ϕ for gas is slightly larger than 90, hence some amount of torque must have been exerted on it from DM. The panels in other columns also lead to similar conclusion.

We now compare the amount of misalignment seen in merger simulations with that of halos simulated in a cosmological context. Bett et al. (2010) show the cumulative misalignment angle with respect to angular momentum vector of material within $r < 0.25 r_{\rm vir}$ while Bailin & Steinmetz (2005) use a differential distribution. We find it much more useful to show the cumulative misalignment with respect to the total angular momentum. In order to see both the inner and outer parts we plot both $\beta(<r)$ and $\beta(>r)$. In addition, we also plot the differential distribution. These are shown in Figure 11. For the range of masses considered here Bett et al. (2010) find a value of around $\beta_{\rm DM-DM}(r < 0.25 r_{\rm vir}) = 25°$ (their Fig 4). The top panel of our figure shows the corresponding quantity to be $30°$ which is in good agreement with their results. Bailin & Steinmetz (2005) plot the orientation profiles with respect to angular different measured in different shells. If the shell at $r = 0.6 r_{vir}$ is taken to be represen-

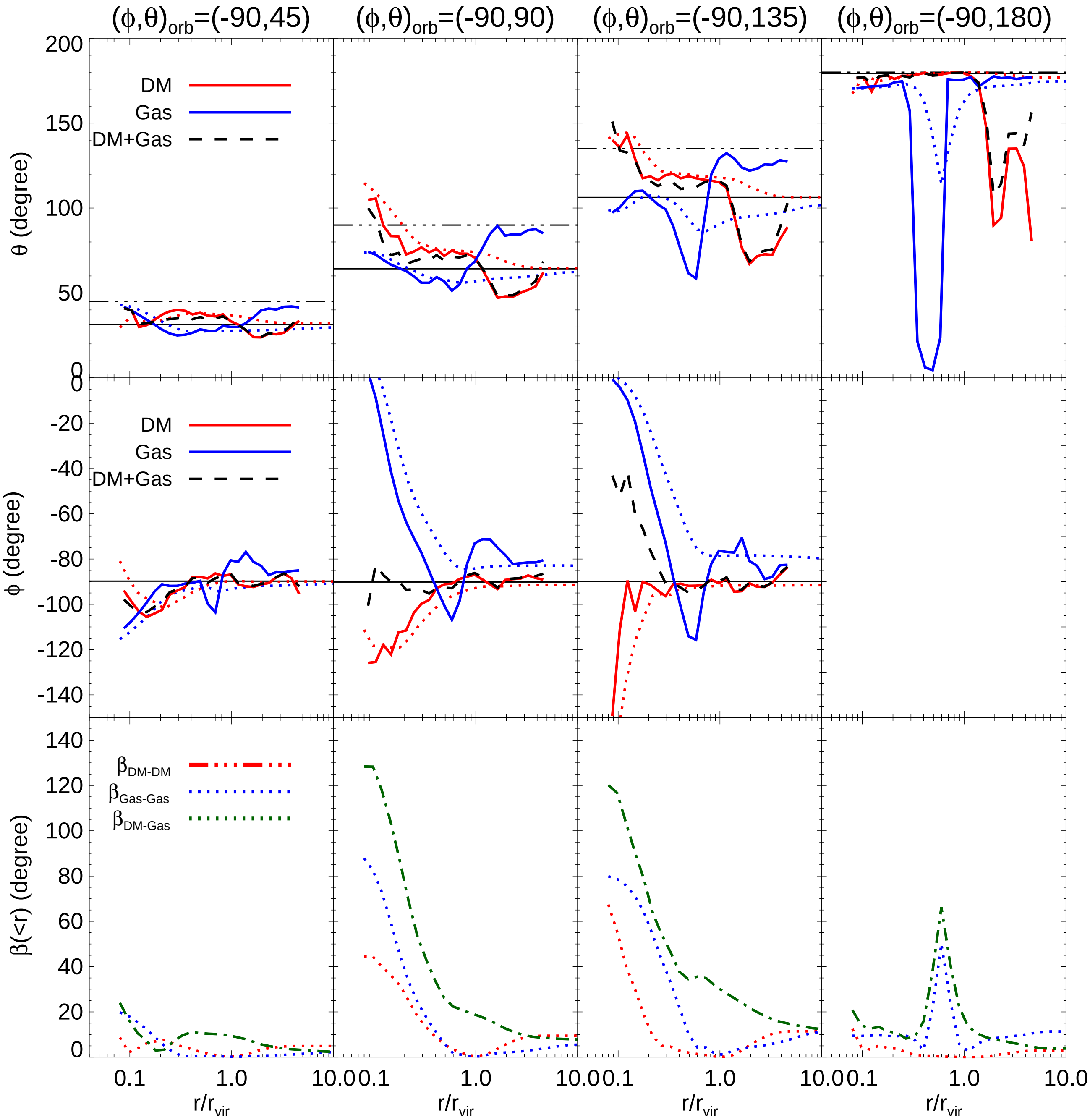

FIG. 10.— Orientation angles θ and ϕ of angular momentum vectors (of gas and dark matter) in a merger in which the initial intrinsic spins of halos where at angle of about $90°$ to the orbital angular momentum of the system. The horizontal black solid line shows the direction of the total angular momentum of the system. The curves were obtained by binning the particles in 25 logarithmically spaced shells. The dotted lines show the cumulative profiles while the solid lines are differential profiles. The dashed line is the differential profile of the whole system (gas and dark matter). The gas and dark matter angular momentum vectors are significantly misaligned with each other, especially in the inner regions. Also in the inner region $r < 0.2r_{\rm vir}$, the angular momentum vectors of gas and dark matter are also individually misaligned with their total angular momentum.

tative of the total angular momentum then this gives a value of about $40°$ and $25°$ for $\beta_{\rm DM-DM}(0.1r_{\rm vir})$ which is again in very good agreement with profile shown in bottom panel of our Figure 11.

We now compare the results of cosmological simulations with that of merger simulations. The trends in top panel are similar to the trends in the second column of bottom row in Figure 10 which corresponds to the most probable orientation of a merger. Figure 11 shows that the median misalignment of gas with respect to dark matter is about $20°$ which is reproduced by Sim 9. Note, higher misalignments can also be achieved if $\theta_{\rm orb}$ is greater than $90°$. The fact that results of the cosmological simulations are successfully reproduced by the merger simulations leads us to conclude that the difference in gas and collisionless dynamics is the main cause of misalignment of angular momentum vectors as seen cosmological simulations. Moreover, misalignments occur only when the intrinsic spins are not aligned with the orbital angular momentum.

Figure 11 also shows that the misalignments are more pro-

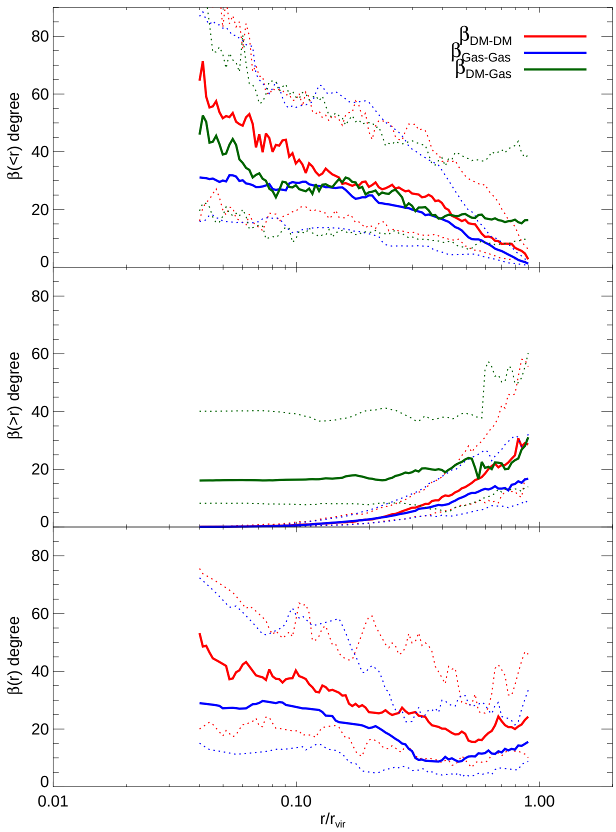

FIG. 11.— Angular momentum orientation profiles of gas and dark matter for halos simulated in cosmological context. The top panel shows the cumulative profile with $\beta(<r) = \hat{\mathrm{j}}(<r).\hat{\mathrm{j}}_{\mathrm{vir}}$, the middle also shows the cumulative profile but for $\beta(>r) = \hat{\mathrm{j}}(>r).\hat{\mathrm{j}}_{\mathrm{vir}}$ and the lower panel shows the differential profile with $\beta(r) = \hat{\mathrm{j}}(r).\hat{\mathrm{j}}_{\mathrm{vir}}$. The angle between angular momentum vectors of gas and dark matter is defined as $\beta_{\mathrm{DM-gas}}(<r) = \hat{\mathrm{j}}_{\mathrm{DM}}(<r).\hat{\mathrm{j}}_{\mathrm{gas}}(<r)$. $\beta_{\mathrm{DM-gas}}(>r)$ also having an analogous definition.

nounced in the inner parts than the outer parts. The fact that the total angular momentum vectors are dominated by the angular momentum in the outer parts is partly responsible for this. Finally, in the orientation profiles of cosmological simulations the dark matter shows more misalignment than the gas whereas the opposite was true for the merger simulations. Given that a real halo has a much more complex merger history than that of a single merger as shown here, we do not consider the discrepancy to be too significant. Moreover there is a significant scatter about the median profiles as shown in Figure 11, which means that on a one to one basis the gas and dark matter can have different trends suggesting that they are sensitive to the merger history and hence could be employed to understand them.

5.6. *Spatial Distribution of low and negative angular momentum material*

The AMD of gas in halos simulated in a cosmological context, shows an excess of low angular momentum material as compared to the AMD required to form an exponential disc. If $s = j/j_{\mathrm{tot}}$ is the specific AM normalized to the mean specific AM, then $0 < s < 0.1$ is the typical region where the theoretical prediction differs from that of exponential discs. Hence we select particles in this range and study their distribution in space. In addition, there is also the issue of material with negative angular momentum, which can arise from two sources. First source is random turbulent motions and second is large scale flows which are remnants of shocks and misaligned minor mergers occurring after the major merger. The negative AM due to the former source would be typically in regions with low AM and would vanish when velocities are smoothed locally, as is done while calculating the AMDs. On the other hand, large scale flows cannot be easily smoothed and is the main reason why Sharma & Steinmetz (2005) find that, in spite of smoothing, cosmological halos have about 8% of matter in negative AM. During the assembly of the disc the negative AM is going to further enhance the fraction of low AM material, hence it is also important to study its distribution in the current context.

In Figure 12 we show the x-z and y-z density maps of low and negative AM gas particles as defined above in various halos. Angular momentum is computed from raw un-smoothed velocities. In the plots the z-axis is aligned with the total angular momentum vector of the halo. The top two rows are for halos from cosmological simulations whereas the lower two rows are for merger simulations. Among these the third row is for a merger where intrinsic spins are misaligned with the orbital AM (Sim 9) and the fourth row is for the fiducial case of an equal mass zero intrinsic spin merger (Sim 1). The plots show that the low angular momentum material is near the center and a conical region around the rotation axis. The negative AM material is also in regions where the AM is low. As discussed earlier in Section 5.1, angular velocity Ω is nearly independent of angle θ and is a decreasing function of radial distance r. In terms of cylindrical radius $R = \sqrt{(r^2 - z^2)}$ the angular momentum is given by ΩR^2. Hence, the angular momentum would be low along the axis of rotation and in the central regions where cylindrical radius R is small. The conical shape is due to the fact that Ω is decreasing function of r. Assuming negative angular momentum is due to random turbulent motions, one expects it to be in regions where $\Omega R/v_{\mathrm{random}}$ is small, which would again be similar to the distribution of low AM material.

For the remnant halo in Sim 1, a part of the negative angular momentum material of gas, is distributed in a ring shaped structure in the y-z plane. During a merger a plane of compressed and shocked gas is formed which is ejected out radially. The ring is created when such a gas which has very low angular momentum falls back at a later time. Note, only about 3% of the gas is in such form which after smoothing reduces to 1%.

The spatial distribution of low AM material has a dependence on the merger history of the halos. For example, in the third row, which is a merger of halos with intrinsic spin misaligned with the orbital AM, the central region looks more puffed up in x-z projection in comparison to the halo in the fourth row. In y-z projection one can see the that the central region is twisted. This appearance is because the AM in the inner regions is misaligned with respect to the total AM. The cosmological halo in the top row also shows such a behavior suggesting a major merger with misaligned spins. The halo in the second row also has slightly twisted axes in the inner region but is very similar to the halo in the bottom row suggesting that the intrinsic spins of its progenitors were either small or well aligned with the orbital AM.

The characteristic distribution of low AM material found in remnant halos as well as cosmological halos suggests that during galaxy formation a mechanism which preferential ejects

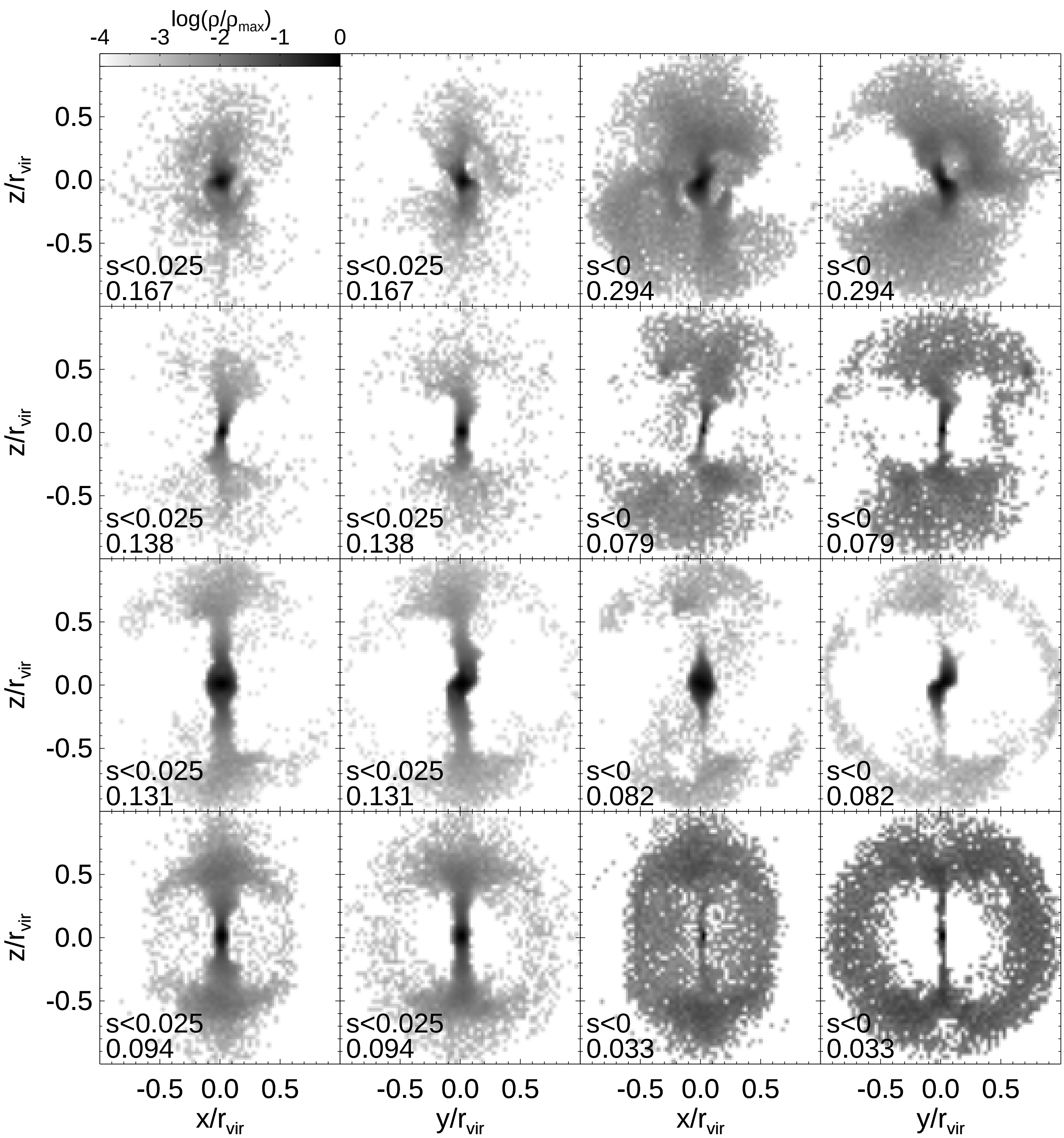

FIG. 12.— Spatial density maps of particles with low AM, i.e., $0 < s < 0.025$ (leftmost two columns) and negative AM, i.e.,$s < 0$) (rightmost two columns) in various halos within the virial radius. Particles are shown in x-y and y-z plane with z axis pointing in the direction of angular momentum. The fraction of low and negative AM particles is also labelled on each plot. The grey scale showing the density maps is normalized to the maximum density in each plot. The top two panels are for halos from cosmological simulations while the lower two panels are for halos formed by merger simulations, namely, Sim 1(third panel) and Sim 9 (fourth panel). The merger simulations results are shown for the final relaxed configuration at $t = 10\ \mathrm{h}^{-1}$ Gyr. Particles with low and negative angular momentum are concentrated in the center and along the axis of rotation.

material from the central regions and prevents further material from collapsing along the rotation axis might alleviate the angular momentum distribution problem. Such preferential ejection might be possible with feedback from star formation. Essentially, the inner parts would collapse first and start forming stars. The feedback would then drive a radial outflow, but since the assembling gas will have a flattened configuration with density being highest near the equatorial regions, the outflow would naturally be stronger along the poles causing preferential ejection of low angular momentum material.

5.7. *Spin up and spin down of halos accompanied by mergers*

It has been reported in earlier studies that immediately after the merger, e.g., the point of pericentric passage, the spin parameter of the dark matter halo is found to be higher and later on as the system virializes the spin is found to drop. To study this we plot in Figure 13 the evolution of spin parameter of gas and dark matter for two merging scenarios, mass fraction $f_m = 0.5$ (Sim 1) and $f_m = 0.1$ (Sim 7). Note, for other

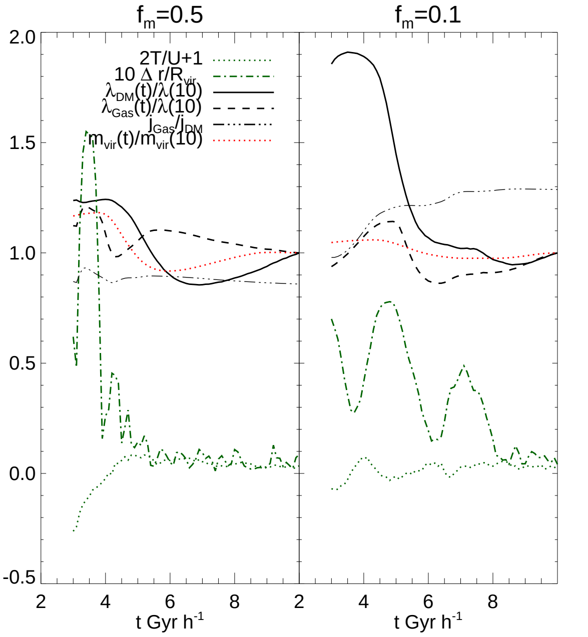

FIG. 13.— Evolution of spin, total angular momentum, offset parameter and the virialization parameter with time. Results are shown for mass ratio $f_m = 0.5$ and 0.1.

merging scenarios the results are quite similar to the Sim 1 case. In both panels $\lambda_{\rm DM}$ is found to drop sharply from the point of first pericentric passage with a slow subsequent rise later on. The evolution of $\lambda_{\rm gas}$ is sensitive to the choice of f_m but in general shows much less variation than that of $\lambda_{\rm DM}$. The drop in $\lambda_{\rm DM}$ for $f_m = 0.5$ case is about 30% whereas for the $f_m = 0.1$ it is about 80%. The sharpest fall of $\lambda_{\rm DM}$ is found to last for about 1 Gyr and occurs between $t = 4$ to $t = 5$ Gyr in the simulations.

Next, we look at the evolution of the ratio $\rm J_{gas}/J_{DM}$. For $f_m = 0.5$, the gas has lost some angular momentum by the time of the start of the merger, but after that the ratio $\rm J_{gas}/J_{DM}$ seems to remain constant. On the other hand, for $f_m = 0.1$ case, the gas is found to gain AM from DM.

Normally, the virialization ratio $2T/U+1$ and the offset parameter defined as $\Delta R/R_{\rm vir}$ is used to detect such non relaxed halos. These are also plotted alongside. Here, T is the kinetic energy and U the potential energy of the system and the offset is defined by $\Delta R = |\mathbf{x}_{\rm cm} - \mathbf{x}_{\rm max\ den}|$. The most commonly used values of these quantities are $-0.5 < 2T/U + 1 < 0.5$ and $\Delta R/R_{\rm vir} < 0.1$. It can be seen from Figure 13 that both these criteria have limited effect in detecting such cases. Our results suggest that a choice of $\Delta R/R_{\rm vir} < 0.025$ should be more effective in detecting such high spin systems.

6. DISCUSSION AND CONCLUSIONS

We have performed hydrodynamical simulations of mergers of spherical halos with a view to understanding the angular momentum properties of halos simulated in a cosmological context. The main angular momentum properties studied include the evolution of angular momentum, the spatial distribution of angular momentum and the orientation of the angular momentum with in the halo. We also explored the differences between the angular momentum properties of gas and dark matter and explain their origin. We now summarize our results and discuss their implications for the formation of disc galaxies.

The shape parameter α of AMDs of gas in merger remnants, is less than one for a wide variety of orbital parameters. This seems to be a generic result of the merging process. Values greater than one and reaching upto 1.08 only occur for unrealistically large value of λ or very low concentration parameter. Lower values of mass ratio f_m and higher values concentration parameter c result in lower value of α . Under the assumption that disks form under conservation of angular momentum this leads to disks that are too centrally concentrated, as exponential disks require a value of α greater than 1.3. In a previous study by Maller & Dekel (2002) it was suggested that halos acquire most of their AM by means of major mergers while minor mergers with small satellites, which come in from random directions, contribute to the low AM material. They argued that by preferentially discarding gas from the shallow potential of these small halos, e.g., by means of supernova feedback, the AM distribution problem could be solved. However, our results show that even in absence of minor mergers, the AMD generated by a major merger has an excess of low angular momentum material. Even the most favorable of merging scenario thus cannot account for the formation of disk galaxies. Indeed, mergers in which the puffing up of gas by feedback was mimiced by decreasing the concentration parameter of the gas, did show a slight increase in value of α, suggesting it might partially help in reducing the low angular momentum material but is not enough to solve the problem.

We find that the angular velocity Ω is almost independent of the spherical co-ordinate θ but exhibits a significant radial gradient. Such behavior is also seen for halos drawn from cosmological simulations. Hence, spherical shells of matter appear to be moving in solid body rotation. This seems like a safe assumption to be used for semi-analytic modelling (van den Bosch 2001, 2002). The spatial distribution of low AM material is found to be in the center and along a conical region along the rotation axis. This suggests that a mechanism which can preferentially eject the material in the center and along the poles can alleviate the angular momentum distribution problem. In fact, feedback from intense star formation in the inner regions can drive such an outflow . Evidence for such an outflow is also provided by observations (Heckman et al. 1990; Shopbell & Bland-Hawthorn 1998; Veilleux & Rupke 2002; Veilleux et al. 2005; Bland-Hawthorn et al. 2007). Essentially, during the formation of the galaxy the star formation will be strongest in the central regions and this will drive an outflow which will expand more along the rotation axis due to the flattened geometry of the assembling gas. This will prevent the rest of the low angular momentum material from falling onto the disc. An idea which was earlier proposed by Sharma (2005)[2] and has also been recently proposed by Brook et al. (2011b). Preferential ejection of low angular momentum material by feedback from the central regions was also used in semi-analytic modelling by (Dutton & van den Bosch 2009; Dutton 2009) to successfully reproduce the exponential structure of discs. The fact that the above process is really responsible for the formation of bulgeless dwarf galaxies has been clearly demonstrated by Brook et al. (2011b) using high resolution cosmological simulations incorporating star formation and feedback. Additionally, as suggested by Brook et al. (2011a), for small mass systems the outflows can eject the low angular momentum material but for large mass systems it can also drive a fountain leading to mixing and redistribution of the low AM material to be accreted later on as high AM

[2] Sec-3 and 5.2 of the PhD thesis

material.

The difference between collisionless dynamics and gas dynamics results in differences between the angular momentum properties of the gas and dark matter and this can potentially have implications for studies that assume them to be same. The gas as compared to dark matter is more efficient in depositing its orbital angular momentum in the central parts of the halo. This results in a higher value of the spin parameter λ for the gas as compared to DM and also a moderately high value of the shape parameter α. Lower values of mass fraction f_m and initial concentration also result in higher $\lambda_{\rm gas}/\lambda_{\rm DM}$ while lower values of $\lambda_{\rm initial}$ and merging time $t_{\rm orb}$ result in lower values of spin ratio. About 6 $\rm h^{-1}$ Gyr after the merger, i.e., the first pericentric passage, the ratio $\lambda_{\rm gas}/\lambda_{\rm DM}$ is found to be greater than 1 for all merging scenarios analyzed here. This seems to be consistent with spin ratios of halos obtained from cosmological simulations at $z = 0$, where $< \lambda_{\rm gas}/\lambda_{\rm DM} >$ is close to 1.4. Using a sample of 14 dwarf galaxies van den Bosch et al. (2001) had found the median spin of galaxies to be 0.06, assuming $\lambda_{\rm DM} = 0.0367$ this gives $\lambda_{\rm gal}/\lambda_{\rm DM} = 1.63$. The fact that we see higher spin for gas might be partly responsible for this but as we discuss later preferential rejection of low angular momentum material during the assembly of the disc is also one of the factors.

We find that for mergers with zero intrinsic spins, the AM vectors of gas and DM are well aligned with misalignment angle being less than $2°$. On the other hand mergers having non-zero intrinsic spins which are inclined at an angle to the orbital AM vector can result in a misalignment of about $20°$, consistent with halos simulated in a cosmological context. Since halos simulated in cosmological context undergo multiple mergers with different spin orientations, the above result provides a natural explanation for this. This shows that the misalignment can be explained purely by means of mergers without any need for the gas and the dark matter to be torqued differently during the formation of the proto-halo. In general, the gas within the virial radius is more effective in retaining the information about the intrinsic spins of the merging halos whereas the dark matter is more effective in retaining the orbital angular momentum information. The misalignment between gas and dark matter has important implications for studies such as, the correlation between the anisotropic distribution of satellite galaxies and the major axis of the central galaxy and weak lensing studies attempting to measure the ellipticity of the dark matter halos.

Mergers with non aligned spins also tend to make the angular momentum of gas as measured in radial shells misaligned with each other. Since galaxies generally form inside out, later infall of misaligned material can cause warps in disc galaxies, and this has recently been shown by Roškar et al. (2010) in cosmological hydrodynamical simulations with star formation. They find that immediately after the major merger the inner gas which forms the disc is misaligned with the rest of the gas in the halo. Later infall of misaligned gas causes the warps. A probable explanation for the cause of misalignment is given by them as the fact that interactions such as minor mergers can affect angular momentum of the inner and outer regions differently. We have here explicitly demonstrated as to how major mergers, in which the orbital angular momentum is not aligned with the intrinsic spin of the halos, generates such a misalignment. Minor mergers later on might further alter the orientation but are not necessarily required to generate the misalignment.

Our results show that the orientation of the angular momentum within the halo depends sensitively upon the orientation of the intrinsic spins of the merging halos with respect to that of the orbital angular momentum. The larger the initial misalignment between the initial angular momentum vectors the larger the final misalignment between the inner and outer parts. This suggests that warps might offer the possibility to probe the merger history of the halo.

Observational evidence for warps is quite ubiquitous (Briggs 1990; Rubin 1994; Sancisi 1976; Verdes-Montenegro et al. 2002). García-Ruiz et al. (2002) find that in their sample of galaxies, all galaxies that have an extended HI disk with respect to the optical are warped. If misalignments in angular momentum are not as frequent then this could pose a problem. Our results show Figure 11 that angular momentum of gas within $r < 0.1r_{\rm vir}$ and $r > 0.9r_{vir}$ is misaligned by more than $10°$, with respect to the total angular momentum vector, for about 84% of the halos (the median misalignments being about $30°$ and $17°$ respectively). This demonstrates that the misalignments are quite common and supports the idea that they are responsible for warps. Just as perfect prograde and perfect retrograde mergers are rare so are systems with small angle warps and systems with counter rotating gas. In future, observations with detailed statistics on the orientation of the warps could be employed to check if they match with the distribution of misalignments predicted by theory.

As mentioned earlier, the amount of misalignment in general is found to increase with the increase of angle between the orbital and intrinsic angular momentum vectors. For retrograde encounters the gas at intermediate radii is even found to be counter rotating. This could be responsible for the counter rotating gas seen in some galaxies. Generally, mergers of gas rich systems are invoked to explain such systems. The quantity of counter rotating gas in some galaxies like NGC3626 is so large that a single minor merger cannot properly account for it. If on the other hand a merger is not minor then it can heat up and thicken the disc considerably . A slow, continuous and well dispersed accretion, as opposed to an accretion via a merging system is preferred (Thakar & Ryden 1996; Ciri et al. 1995). Counter rotating gas in galactic halos formed by retrograde mergers as shown here, naturally provides such an extended reservoir of gas. A recent merger which can potentially heat up the disc is not required, the counter rotating gas is formed early on during the last major merger, which causes the inner and outer regions to rotate in different directions. In such a scenario, the inner regions first assemble to form the disc, rest of the material falls later on to generate the counter rotating gas.

We also studied the issue of spin up of a halo undergoing a merger and the subsequent spin down during virialization (Gardner 2001; Vitvitska et al. 2002; Peirani et al. 2004; Hetznecker & Burkert 2006). As argued by D'Onghia & Navarro (2007), in collisionless mergers central regions tend to be populated by low angular momentum material and high angular momentum material is pushed to weakly bound orbits. When angular momentum is measured with the fixed radius like the virial radius the effect is a spin down. Our merger simulations also show a similar effect. For dark matter the inner half loses angular momentum while the outer half gains. The main cause for such a redistribution of angular momentum is the collisionless dynamics and is as follows. For dark matter during the collision the late in-falling particles have high angular momentum and high energy and they gain energy during the collapse and hence can easily climb out of the final relaxed potential which is much shallower. Hence, high angular momentum particles get pushed to weaker and weaker orbits making them move outwards. For gas the late in-falling particles shock and deposit their angular momentum onto the inner regions making them behave differently. We find that for a Milky Way sized halo the spin down process lasts about a giga year, and the spin of dark matter can fall by about $40-80\%$ during this time, depending mainly upon the mass ratio of the merging components. The spin of gas shows somewhat less variation. We find that the virial ratio $2T/U+1$ is not very effective in detecting such situations. The offset parameter is more successful in detecting such cases but a value of $\Delta R/R_{\rm vir}<0.025$ would be needed, which is much less than what is currently used (D'Onghia & Navarro 2007; Neto et al. 2007). Hence, recent results showing high spin systems to be more clustered might be affected by this bias (Bett et al. 2007; Davis & Natarajan 2010). Alternatively, it might reflect the fact that in clustered environments mergers and hence non relaxed halos are more common. If non relaxed halos is the cause of correlation between the clustering and spin then the ability to observationally detect it by measuring spin of galaxies is unclear, as galaxies form out of baryons in relaxed halos. Additionally, it is not known if the spin of baryons would also show such a clustering.

Finally, our results show that mergers of NFW halos naturally generate the universal form of angular momentum distributions as seen in simulations. For dark matter the value of the shape parameter α is in excellent agreement with the results from cosmological simulations. However, this does not mean that mergers are the only way to generate such distributions. As has been shown recently by Wang & White (2009) even hot dark matter simulations which have almost no mergers show such angular momentum distributions. Hence, the origin of the universal form is more generally related to the virialization processes such as the violent relaxation. However, our results show that mergers do induce subtle differences between the angular momentum properties of dark matter and gas. The alignment of the angular momentum vector with in the halo and also that of gas with respect to dark matter is sensitively related to the merger history and might serve to discriminate the dark matter models. In hot dark matter models, although less likely, but misalignments as discussed above could also be produced if matter coming from different regions have angular momentum pointing in different directions.

ACKNOWLEDGMENTS

This work has been supported by grants from the U.S. National Aeronautics and Space Administration (NAG 5-10827), the David and Lucile Packard Foundation. SS is funded through ARC DP grant 0988751 which supports the HERMES project. JBH is funded through a Federation Fellowship from the Australian Research Council (ARC). A part of the research was undertaken on the NCI National Facility in Canberra, Australia, which is supported by the Australian Com-

REFERENCES

Agustsson, I., & Brainerd, T. G. 2006, ApJ, 650, 550
Avila-Reese, V., Firmani, C., & Hernández, X. 1998, ApJ, 505, 37
Azzaro, M., Patiri, S. G., Prada, F., & Zentner, A. R. 2007, MNRAS, 376, L43
Bailin, J., & Steinmetz, M. 2005, ApJ, 627, 647
Baugh, C. M., Cole, S., & Frenk, C. S. 1996, MNRAS, 283, 1361
Benson, A. J., Bower, R. G., Frenk, C. S., Lacey, C. G., Baugh, C. M., & Cole, S. 2003, ApJ, 599, 38
Bett, P., Eke, V., Frenk, C. S., Jenkins, A., Helly, J., & Navarro, J. 2007, MNRAS, 376, 215
Bett, P., Eke, V., Frenk, C. S., Jenkins, A., & Okamoto, T. 2010, MNRAS, 404, 1137
Binney, J., & Tremaine, S. 2008, Galactic Dynamics: Second Edition (Princeton University Press)
Bland-Hawthorn, J., Veilleux, S., & Cecil, G. 2007, Ap&SS, 311, 87
Bland-Hawthorn, J., et al. 2011, Optics Express, 19, 2649
Blumenthal, G. R., Faber, S. M., Flores, R., & Primack, J. R. 1986, ApJ, 301, 27
Brainerd, T. G. 2005, ApJ, 628, L101
Briggs, F. H. 1990, ApJ, 352, 15
Brook, C. B., Stinson, G., Gibson, B. K., Roškar, R., Wadsley, J., & Quinn, T. 2011a, ArXiv e-prints
Brook, C. B., et al. 2011b, MNRAS, 595
Bryan, G. L., & Norman, M. L. 1998, ApJ, 495, 80
Bryant, J. J., O'Byrne, J. W., Bland-Hawthorn, J., & Leon-Saval, S. G. 2011, MNRAS, 797
Bullock, J. S., Dekel, A., Kolatt, T. S., Kravtsov, A. V., Klypin, A. A., Porciani, C., & Primack, J. R. 2001, ApJ, 555, 240
Chen, D. N., Jing, Y. P., & Yoshikaw, K. 2003, ApJ, 597, 35
Ciri, R., Bettoni, D., & Galletta, G. 1995, Nature, 375, 661
Cole, S., Aragon-Salamanca, A., Frenk, C. S., Navarro, J. F., & Zepf, S. E. 1994, MNRAS, 271, 781
Dalcanton, J. J., Spergel, D. N., & Summers, F. J. 1997, ApJ, 482, 659
Davis, A. J., & Natarajan, P. 2010, MNRAS, 407, 691
D'Onghia, E., & Navarro, J. F. 2007, MNRAS, 380, L58
Dutton, A. A. 2009, MNRAS, 396, 121
Dutton, A. A., & van den Bosch, F. C. 2009, MNRAS, 396, 141
Dutton, A. A., van den Bosch, F. C., Dekel, A., & Courteau, S. 2007, ApJ, 654, 27
Fall, S. M., & Efstathiou, G. 1980, MNRAS, 193, 189
García-Ruiz, I., Sancisi, R., & Kuijken, K. 2002, A&A, 394, 769
Gardner, J. P. 2001, ApJ, 557, 616
Gnedin, O. Y., Weinberg, D. H., Pizagno, J., Prada, F., & Rix, H.-W. 2007, ApJ, 671, 1115
Governato, F., et al. 2010, Nature, 463, 203
Heckman, T. M., Armus, L., & Miley, G. K. 1990, ApJS, 74, 833
Hetznecker, H., & Burkert, A. 2006, MNRAS, 370, 1905
Kang, X., Jing, Y. P., Mo, H. J., & Börner, G. 2005, ApJ, 631, 21
Kang, X., van den Bosch, F. C., Yang, X., Mao, S., Mo, H. J., Li, C., & Jing, Y. P. 2007, MNRAS, 378, 1531
Kauffmann, G. 1996, MNRAS, 281, 475
Kauffmann, G., Colberg, J. M., Diaferio, A., & White, S. D. M. 1999, MNRAS, 303, 188
Kauffmann, G., & Haehnelt, M. 2000, MNRAS, 311, 576
Kazantzidis, S., Magorrian, J., & Moore, B. 2004, ApJ, 601, 37
Macciò, A. V., Dutton, A. A., van den Bosch, F. C., Moore, B., Potter, D., & Stadel, J. 2007, MNRAS, 378, 55
Maller, A. H., & Dekel, A. 2002, MNRAS, 335, 487
Maller, A. H., Dekel, A., & Somerville, R. 2002, MNRAS, 329, 423
Mo, H. J., Mao, S., & White, S. D. M. 1998, MNRAS, 295, 319
Navarro, J. F., & Benz, W. 1991, ApJ, 380, 320
Navarro, J. F., Frenk, C. S., & White, S. D. M. 1996, ApJ, 462, 563
—. 1997, ApJ, 490, 493
Navarro, J. F., & Steinmetz, M. 1997, ApJ, 478, 13
Navarro, J. F., & White, S. D. M. 1994, MNRAS, 267, 401
Neto, A. F., et al. 2007, MNRAS, 381, 1450
Nichols, M., & Bland-Hawthorn, J. 2009, ApJ, 707, 1642
—. 2011, ApJ, 732, 17
Peebles, P. J. E. 1969, ApJ, 155, 393
Peirani, S., Mohayaee, R., & de Freitas Pacheco, J. A. 2004, MNRAS, 348, 921
Roškar, R., Debattista, V. P., Brooks, A. M., Quinn, T. R., Brook, C. B., Governato, F., Dalcanton, J. J., & Wadsley, J. 2010, MNRAS, 408, 783
Rubin, V. C. 1994, AJ, 108, 456
Sancisi, R. 1976, A&A, 53, 159
Sharma, S. 2005, PhD thesis, The University of Arizona, Arizona, USA
Sharma, S., & Steinmetz, M. 2005, ApJ, 628, 21
Shopbell, P. L., & Bland-Hawthorn, J. 1998, ApJ, 493, 129
Sil'chenko, O. K., & Moiseev, A. V. 2006, AJ, 131, 1336
Sil'chenko, O. K., Moiseev, A. V., & Afanasiev, V. L. 2009, ApJ, 694, 1550

Somerville, R. S., & Primack, J. R. 1999, MNRAS, 310, 1087
Sommer-Larsen, J., Gelato, S., & Vedel, H. 1999, ApJ, 519, 501
Springel, V., Yoshida, N., & White, S. D. M. 2001, New Astronomy, 6, 79
Steinmetz, M., & Navarro, J. F. 1999, ApJ, 513, 555
Thakar, A. R., & Ryden, B. S. 1996, ApJ, 461, 55
van den Bosch, F. C. 2000, ApJ, 530, 177
—. 2001, MNRAS, 327, 1334
—. 2002, MNRAS, 332, 456
van den Bosch, F. C., Abel, T., Croft, R. A. C., Hernquist, L., & White, S. D. M. 2002, ApJ, 576, 21
van den Bosch, F. C., Burkert, A., & Swaters, R. A. 2001, MNRAS, 326, 1205
Veilleux, S., Cecil, G., & Bland-Hawthorn, J. 2005, ARA&A, 43, 769
Veilleux, S., & Rupke, D. S. 2002, ApJ, 565, L63
Verdes-Montenegro, L., Bosma, A., & Athanassoula, E. 2002, A&A, 389, 825
Vitvitska, M., Klypin, A. A., Kravtsov, A. V., Wechsler, R. H., Primack, J. R., & Bullock, J. S. 2002, ApJ, 581, 799
Wang, J., & White, S. D. M. 2009, MNRAS, 396, 709
Wang, Y., Yang, X., Mo, H. J., Li, C., van den Bosch, F. C., Fan, Z., & Chen, X. 2008, MNRAS, 385, 1511
White, S. D. M. 1984, ApJ, 286, 38
White, S. D. M., & Rees, M. J. 1978, MNRAS, 183, 341
Yang, X., van den Bosch, F. C., Mo, H. J., Mao, S., Kang, X., Weinmann, S. M., Guo, Y., & Jing, Y. P. 2006, MNRAS, 369, 1293